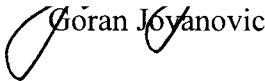


AN ABSTRACT OF THE THESIS OF

Brian Kanghee Rhee for the degree of Master of Science in Chemical Engineering
presented on February 18, 1998. Title : Enhancement of Mass Transfer Coefficient in
three-phase Magnetically Stabilized Fluidized Bed.

Abstract approved : _____ **Redacted for Privacy** _____
 _____

The correlations for a liquid-solid mass transfer coefficient at different operating conditions are well known for the conventional two-phase and three-phase fluidized bed. However, no correlation is found for the liquid-solid mass transfer coefficient when a uniform magnetic field is applied in a three-phase fluidized bed of ferromagnetic particles ($d_p = 3 \text{ mm}$, $\rho_p = 1.515 \text{ g/cm}^3$, 20 % of ferromagnetic material).

The enhancement of mass transfer coefficient in a three-phase Magnetically Stabilized Fluidized Bed (MSFB) is experimentally observed. The adsorption of the methylene blue dye on the ferromagnetic particles is the technique used in this study. Two operating conditions, gas velocity (0-1.17 cm/s) and the magnetic field (0-11.7 kA/m), are varied. It is confirmed that the increase of the magnetic field, as well as the increase of the gas velocity results in up to 250 % higher mass transfer coefficient in the experimental range. The prime reason for the improved mass transfer rate with the application of the magnetic field is the increase of the fluid interstitial velocity, which is caused by the decrease of the

liquid porosity, and the structural change of the bed itself due to interparticle forces induced by the magnetic field.

As a final result, the emperical correlation

$$Sh = 0.01224(Ed_p^4/\nu_l^3)^{0.45} Sc^{1/3}$$

where E, the energy dissipation

$$E = g\{(u_l + u_g)(\epsilon_s \rho_p + \epsilon_l \rho_l) - u_l \rho_l + 0.12H\}/(\epsilon_l \rho_l)$$

is derived. Newly defined Energy dissipation term E was introduced to explain the effect of the two changing factors, gas flow and magnetic field.

Liquid porosity in the above correlation is derived from a modified equation first proposed by Honorez (1994),

$$\epsilon_l = \epsilon_{l,ms} + (\epsilon_{l,ff} - \epsilon_{l,ms}) \exp(-(1 - \epsilon_l)(\alpha H + \beta) \frac{H}{H_{ms}})$$

This equation can be used if the magnetic field doesn't affect the gas porosity in the bed.

A mathematical model was developed and solved analytically to evaluate the mass transfer coefficient from the experimental data.

$$\ln\left\{\frac{C(1 + mK_e) - C_0}{C_0(1 + mK_e) - C_0}\right\} = \frac{1 + mK_e}{mK_e} \frac{F}{V} (e^{-\alpha k} - 1)t$$

**Enhancement of Mass Transfer Coefficient
in
three-phase Magnetically Stabilized Fluidized Bed**

by

Brian Kanghee Rhee

A THESIS

submitted to

Oregon State University

**in partial fulfillment of
the requirement for the
degree of**

Master of Science

**Completed February 18, 1998
Commencement June 1998**

Master of Science thesis of Brian K. Rhee presented on February 18, 1998

APPROVED:

Redacted for Privacy

Major Professor, representing Chemical Engineering

Redacted for Privacy

Head of Department of Chemical Engineering

Redacted for Privacy

Dean of the Graduate School

I understand that my thesis will become part of the permanent collection of Oregon State University libraries. My signature below authorizes release of my thesis to any reader upon request.

Redacted for Privacy

Brian K. Rhee, Author

TABLE OF CONTENTS

	<u>Page</u>
CHAPTER 1 - INTRODUCTION	1
CHAPTER 2 - EXPERIMENTAL APPARATUS	3
2.1 - Fluidization Column	3
2.2 - Fluidizing Particles	5
2.3 - Water and Air Supply System	7
2.4 - Instrumentation	7
2.5 - The Magnetic Field Generator	8
CHAPTER 3 - THEORETICAL BACKGROUND	10
3.1 - Liquid-Solid Mass transfer Coefficient in Fluidized Beds	10
3.2 - Mathematical Model for the Adsorption in three-phase MSFB	15
CHAPTER 4 - EXPERIMENTAL MEASUREMENTS	23
4.1 - Adsorption Isotherm	23
4.2 - The Height and Porosity of the Bed	26
4.3 - Measurements of the MB Concentration in three-phase MSFB	30

TABLE OF CONTENTS (Continued)

	<u>Page</u>
CHAPTER 5 - EXPERIMENTAL RESULTS AND DISCUSSION	31
5.1 - The Average Porosity of the Liquid and the Gas Phase	31
5.2 - Mass Transfer Coefficient Calculation	34
5.3 - Mass Transfer Coefficient Correlation	42
CHAPTER 6 - CONCLUSION AND RECOMMENDATION	48
6.1 - Conclusion	48
6.2 - Recommendations	50
BIBLIOGRAPHY	51
APPENDICES	54
A - The Design of the Distributor Plate	55
B - Particles Production	56
C - The Colorimeter Calibration Curve	60
D - The Voltage vs. Current Calibration Curve	61
E - The Numerical Method for solving the Mathematical Model	62
F – Diffusion Coefficient Calculation from Numerical Method	69
G - Analytical Solution for the Model	70
H - Dynamic Pressure at Each Port	72
I - Concentration Measurements	73
J - Calculation of the Diffusion Coefficient of MB into water	77

LIST OF FIGURES

<u>Figure</u>	<u>Page</u>
2-1 The Experimental Apparatus	4
2-2 Ferromagnetic Composite Particles	5
3-1 Balance of Forces	14
3-2 Combining Effect of the Gas Agitation and the Magnetic Field	16
3-3 The Experimental System and the Model	17
4-1 Adsorption Isotherm Plot	25
4-2 Determination of the Bed Height L	28
4-3 Axial Dynamic Pressure at $H=4.28$ kA/m and Liquid Velocity 5cm/s	29
5-1 Average Porosities as a Function of Magnetic Field for Different Gas Velocities	32
5-2 Determination of the Initial Slope S	36
5-3 Mass Transfer Coefficient k as a Function of H for Different Gas Velocity	39
5-4 Mass Transfer Coefficient k as a Function of Gas Velocity for Different H	40
5-5 Comparison of This Work with Other Published Data on k in Three-phase Fluidized Beds and in Packed Beds with Gas-Liquid Upflow	43
5-6 Possibility of Introducing the New Term in Energy Dissipation E	44
5-7 Correlation of the Mass Transfer Coefficient k with Magnetic Field H	46
5-8 Sh from the Experiment versus Sh from Correlation Prediction	47
B-1 Extrusion of the Particles	57

LIST OF TABLES

<u>Table</u>	<u>Page</u>
2-1 Pressure Port Locations along the Fluidization column	8
3-1 Liquid-Solid Mass Transfer Correlations	11
4-1 Adsorption Isotherm Data	24
4-2 The Bed Heights and Calculated Porosities Data	30
5-1 Measured k Values for Different Gas Velocities and Different Magnetic Field Intensities	38
B-1 Ferrite and Alginate Properties	59
I-1 MB Concentration Measurement at $u_f = 5$ cm/s and $H = 0$ kA/m	73
I-2 MB Concentration Measurement at $u_f = 5$ cm/s and $H = 4.28$ kA/m	74
I-3 MB Concentration Measurement at $u_f = 5$ cm/s and $H = 7.71$ kA/m	75
I-4 MB Concentration Measurement at $u_f = 5$ cm/s and $H = 11.2$ kA/m	76

NOMENCLATURE

A	cross section of the column	$[cm^2]$
a	the outer surface of the particles	$[cm^2]$
a'	the outer surface of particles per unit volume of the bed	$[cm^{-1}]$
C	concentration of MB in the liquid in system boundary (1)	$[g/cm^3]$
C'	concentration of MB in the liquid coming out of the bed	$[g/cm^3]$
C^*	concentration of MB in bulk liquid in system boundary(2)	$[g/cm^3]$
C_s	concentration of MB in liquid at $r=R$	$[g/cm^3]$
C_{ss}	steady state concentration of MB	$[g/cm^3]$
C_r	concentration of MB in liquid-filled pore at radius r	$[g/cm^3]$
C_0	concentration of MB in bulk liquid at start of adsorption run	$[g/cm^3]$
d_p	average particle diameter	$[cm]$
D	diffusion coefficient	$[cm^2/s]$
D_e	total effective diffusion coefficient in particles	$[cm^2/s]$
E	the energy dissipated per unit mass of liquid	$[s^3/cm^2]$
F	liquid flow rate	$[cm^3/s]$
F_b	bouyant force	$[N]$
F_d	drag force	$[N]$
F_g	gravitational force	$[N]$
F_m	magnetic force	$[N]$

H	magnetic field intensity	[kAturns/m]
H_{ms}	magnetic field intensity at the transition from the partially stabilized to stabilized regime	[kAturns/m]
I	Electric Current	[A]
k	liquid-solid mass transfer coefficient	[cm/s]
K_e	adsorption equilibrium constant	[cm ³ / g of particles]
L	effective bed height	[cm]
L_0	bed height when bed is packed	[cm]
M	the mass of particles	[g]
m	mass of particles per unit volume of particle-free slurry	[g/cm ³]
n	number of copper coil turns per meter length of column	[turns/m]
N	concentration of adsorbed MB at radius r on the particles [g of MB/g of particles]	
P	pressure	[Pa]
P_d	dynamic pressure	[Pa]
R	average particle radius	[cm]
r	radial coordinate in a particle	[cm]
Re	Reynolds number = $\frac{d_p u_l \rho_l}{\mu_l} = \frac{d_p u_l}{\nu_l}$	[/]
S	the slope in Figure 5-2	[1/s]
Sc	Schmidt number = $\frac{\mu_l}{\rho_l D} = \frac{\nu_l}{D}$	[/]
Sh	Sherwood number = $\frac{k d_p}{D}$	[/]
t	time	[sec]

u_g	the gas velocity	[cm/s]
u_l	the superficial liquid velocity	[cm/s]
$u_{l,int}$	the interstitial liquid velocity	[cm/s]
V	the volume of the system not including the bed	[cm^3]
V_L	the overall volume of the system	[cm^3]
W_s	total mass of the solid particles	[g]
x	axial coordinate in the bed	[cm]

Greek symbols

α	constant in equation (3-11), $= \frac{\alpha' AL}{F}$	[cm^{-1}]
α	constant in equation (3-5) and (5-2)	
β	constant in equation (3-5) and (5-2)	
ε	the sum of the gas and liquid porosity $= \varepsilon_g + \varepsilon_l = 1 - \varepsilon_s$	[/]
ε_{ff}	the liquid porosity when $H=0$	[/]
ε_g	the porosity of the gas in the bed = the volume fraction of the gas phase in the bed	[/]
ε_l	the porosity of the liquid in the bed = the volume fraction of the liquid phase in the bed	[/]
$\varepsilon_{l,0}$	the porosity of the liquid when bed is packed	[/]
ε_{ms}	the porosity of the liquid at the transition from the partially stabilized to stabilized regime	[/]
ε_p	voidage inside the particles	[/]

ε_s	the porosity of the solid particles in the bed = the volume fraction of the solid particles in the bed	[/]
ρ_g	density of the gas	[g/cm ³]
ρ_l	density of the liquid	[g/cm ³]
ρ_p	density of particles	[g/cm ³]
$\Re(C_r)$	generation rate of MB	[g of MB/(cm ³ pore × s)]
ν_l	kinematic viscosity of the liquid	[cm ² / s]
ψ	constant in equation (5-11)	[kg / kA · m · s]

Enhancement of Mass Transfer Coefficient in three-phase Magnetically Stabilized Fluidized Bed

CHAPTER 1 INTRODUCTION

Gas-liquid-solid three-phase fluidized beds have been used for various industrial processes including physical, chemical, petrochemical, electrochemical, and biochemical operations. The performance of the three-phase fluidized-bed reactor in these processes often depends on the rate of mass and heat transfer between solid particles and a liquid.

A Magnetically Stabilized Fluidized Bed (MSFB) is a recent and novel chemical engineering development in the area of fluid-solid contacting operations including gas-liquid-solid three-phase fluidization systems. It combines some of the best characteristics of fluidized beds, like low pressure drop and the ability to transport solid throughout the system, with excellent efficiency of the fixed beds in mass transfer, heat transfer and chemical conversion.

Fluid-particle mass transfer in fluidized beds is a very important transport phenomenon in many chemical engineering operations such as adsorption, desorption, drying, ion exchange and evaporation. Numerous studies have been conducted on the mass transfer coefficient between liquid and solid. However, only some of them, Kikuchi et al.(1983), Arters and Fan (1986), Fukuma et al.(1988) were performed in a three-phase fluidized bed. None of the above references address the possibility of using additional nontraditonal forces (magnetic, electric etc.) toward enhancement of mass

transfer coefficient k . Al-Mulhim and Jovanovic (1995) showed the enhancement of mass transfer coefficient in a liquid-solid two-phase fluidized bed when a magnetic field is applied on the bed of ferromagnetic particles. However, there is no data in the literature showing the influence of the magnetic field in the liquid-solid mass transfer in a three-phase MSFB.

In the present work, air, methylene blue solution and ferromagnetic particles are employed as three phase to study the enhancement of the mass transfer coefficient in three-phase MSFB. The main objective of this work is to study the combining effect of the magnetic field and the gas velocity on the mass transfer coefficient between water and ferromagnetic particles in a three-phase MSFB. To accomplish this objective, the following tasks had to be accomplished.

- 1-design and construction of the experimental apparatus including a two-phase distributor plate,
- 2-production of ferromagnetic particles,
- 3-collection of experimental data on the effect of magnetic field intensity on bed voidage(porosity),
- 4-measurement of porosities of each phase,
- 5-development of a representative mathematical model to calculate mass transfer coefficients.

As a final results, a correlation for mass transfer coefficient in terms of porosities of the liquid and gas phase, which are affected by the magnetic field intensity, as well as the flow of the liquid and gas, is established. In the process, some of the hydrodynamic characteristics of the three- phase MSFB were determined.

CHAPTER 2

EXPERIMENTAL APPARATUS

A schematic representation of the experimental apparatus used in this study is shown in Figure 2-1. The apparatus consists of five major elements:

- 1 - the fluidization column,
- 2 - the fluidizing particles
- 3 - the water and air supply system,
- 4 - instrumentation,
- 5 - the magnetic field generator.

2.1 Fluidization Column:

The column in which the particles are fluidized is made of Plexiglas, allowing visual observation through the wall. It is assembled from two removable parts: a calming section at the bottom, followed by the fluidization column, a 670 mm long pipe, 52 mm internal diameter, which fits into the calming section. A distributor plate is located inside the pipe and it can be easily relocated or removed. The fluid distributor plate is shown in Appendix A. It is 52 mm in diameter and has forty four 2 mm circular holes for liquid distribution and twenty five 300 μ holes for gas distribution. The two-phase distributor plate is very important part in the design and operation of the experiment. Eight pressure ports on the column wall are used for pressure measurements. (For details, see section 2.4. Instrumentation) The bed is operated at room temperature and atmospheric pressure.

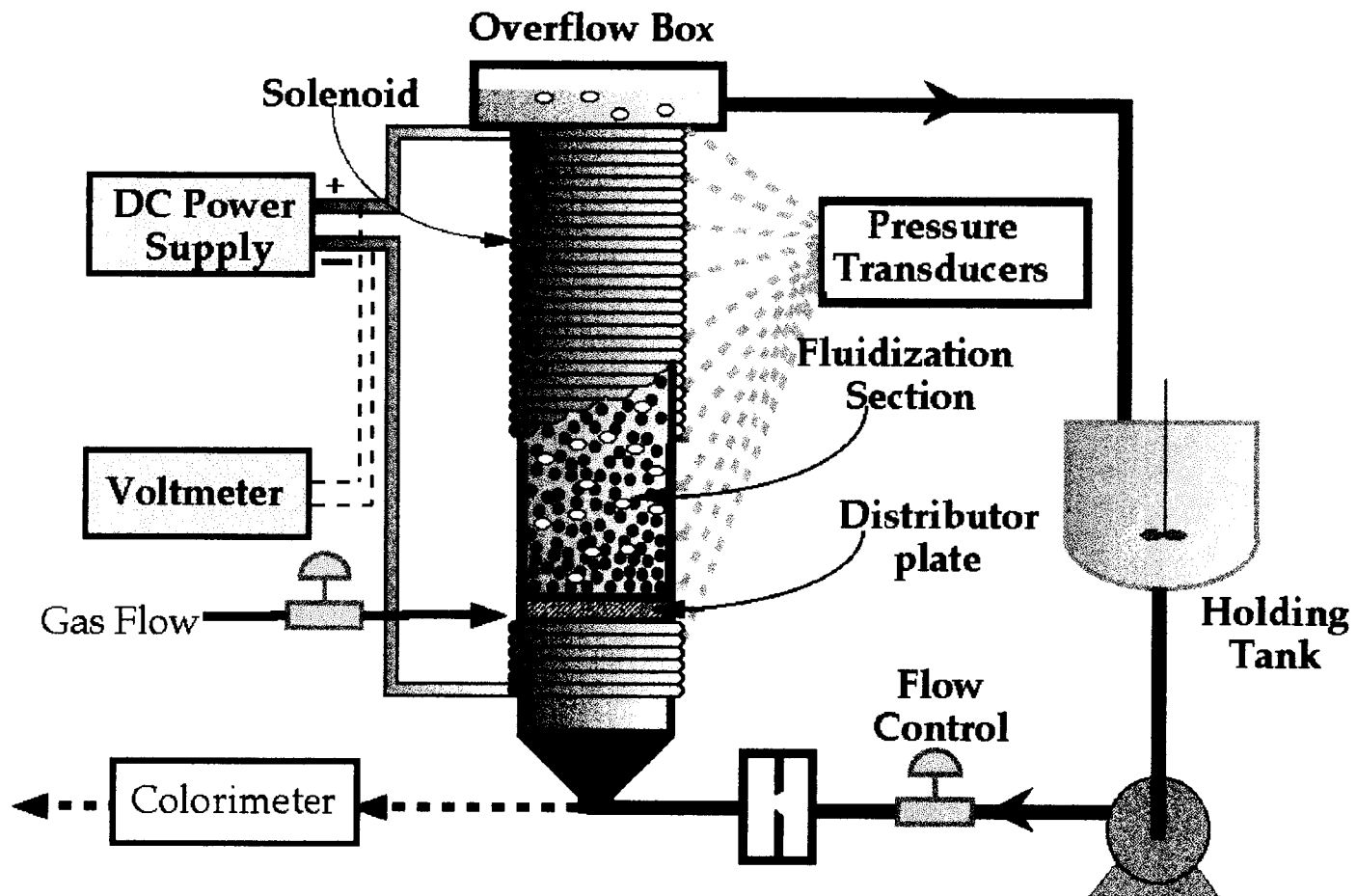


Figure 2-1 Experimental Apparatus

2.2 Fluidizing Particles:

2.2.1 Particles Production

The particles used in this study are composite ferromagnetic particles which are made of alginate mixed with ferromagnetic powder and activated carbon.

(Figure 2-2)

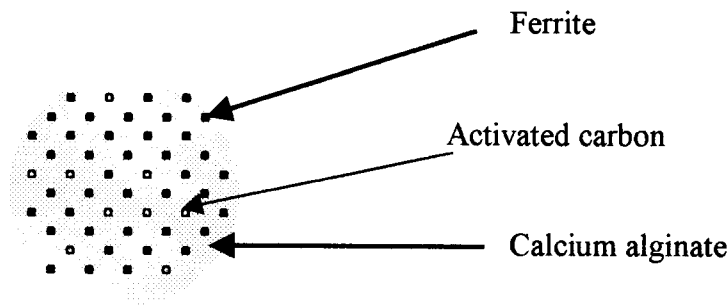


Figure 2-2: Ferromagnetic composite particles

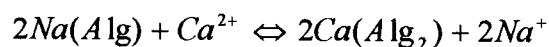
An air assisted particle generator is used for the production of the particles. It is schematically shown in Figure B-1 in Appendix B.

Ferromagnetic Alginate Mixture Suspension : A 1.75% (by weight) solution of high viscosity (Kelton HV donated by Kelco Co.) sodium alginate in DI water is prepared beforehand and then, the ferromagnetic powders and activated carbon powders are added, 20% and 10% (by weight) respectively. This mixture suspension is prepared according to the procedure described in Appendix B. The properties of the alginate sodium and ferromagnetic powder (Steward Ferrites -Chattanooga, Tennessee, USA) are also listed in

Appendix B (Table B-1). The suspension should be mixed continuously to prevent powder precipitation from the suspension.

The Particle Generation: The alginate-ferrite-activated suspension prepared goes into the device shown in Figure B-1 in Appendix B and comes out of the nozzle where droplets are formed. The particle size can be adjusted by regulating the flow rate of the suspension and the air flow, which is used to shear the particles off the dripper nozzle. (For more details, see Haas (1975) or Appendix B)

Calcium Chloride Cross-linking Solution : A 1.0 Molar calcium chloride solution is used to cross link the ferromagnetic sodium alginate droplets coming out of the dripper. Once the droplets are introduced to the calcium chloride solution, almost instantly calcium alginate will form on the surface of the sodium alginate beads and they will maintain their spherical shape which they had when injected into the calcium chloride solution. Initially, the bead center will be non polymerized sodium alginate, but over a short period of time calcium will diffuse into the center and form a calcium alginate structure throughout the bead. The reaction between calcium ions and the alginate molecules can be represented by:



The composite ferromagnetic droplets are left in calcium chloride solution for 60 minutes before they are ready for use.

2.2.2 Particles Properties

The mean diameter of the particles is 3mm and their density is 1.515 g/cm^3 . The density of the particles is determined from volumetric and weight measurements in water.

2.3 Water and Air Supply System:

DI water and air were used for liquid and gas phase respectively. The water and air flow rate were measured by an orifice meter installed in the supply line. Water flow rate is fixed at 5cm/s and air flow rate is varied from 0 to 1.172cm/s. Any desired flow rate of air can be adjusted by control valve.

2.4 Instrumentation:

2.4.1 The dynamic pressure measuring system

The dynamic pressure (See Chapter 4 for definition) measuring system consists of a bank of seven piezometric glass tubes, 4mm in diameter. Each of them is connected to its corresponding pressure port mounted on the column wall. Each pressure port is covered with plastic wire-mesh screen to prevent particles from entering the tubes. The locations of the pressure ports along the fluidization column are given in Table 2-1.

Table 2-1 Pressure port locations along the fluidization column

Port #	Distance (cm above the distributor plate)
1	3.2
2	8.4
3	13.4
4	18.5
5	23.5
6	28.6
7	33.7
8	38.7

2.4.2 Colorimeter

Methylene blue (MB) dye is used as the adsorbate substance in this work. Spectronic 20 (Bausch and Lomb) is used to measure the absorbance of the MB dye. Beer-Lambert law indicates that the absorbance is linearly proportional to the corresponding MB concentrations. The instrument is calibrated and calibration curve is shown in Appendix C.

2.5 The Magnetic Field Generator:

The magnetic field generator consists of two direct current (DC) power supplies connected in series with a copper coil solenoid. The solenoid consists of 90 turns of 4 mm diameter copper tubing that is fixed around a 10.2[cm] outer diameter and 46 cm long plastic tube. This is equivalent to 195.65 turns per meter length of column.

$$n = 195.65 \text{ [turns/m]}$$

Each DC power supply could maintain a 0-5[V] voltage across the solenoid. Cooling water was passed through the solenoid to prevent it from overheating. The output voltage of the DC power supplies, and hence the corresponding current through the solenoid, was manually controlled using a voltage control knob. To determine the system resistance, the setting of the power supply was controlled manually, and the voltage readings and their corresponding current readings were recorded. The system resistance was found to be 0.0731Ω . The voltage vs. current calibration curve is shown in Appendix D.

The magnetic field intensity H can be calculated according to the following relation:

$$H = I \times n \text{ [A/m]}$$

where I is the electric current and n the number of turns per length of column in the solenoid.

CHAPTER 3 THEORETICAL BACKGROUND

3.1 Liquid-Solid Mass Transfer Coefficient in Fluidized Beds:

Numerous studies have been performed in various fluidized bed systems to correlate liquid-solid mass transfer coefficient with the operating variables and physical properties of the individual phases. Table 3-1 summarizes the existing correlations between liquid-solid mass transfer coefficient (contained in Sherwood number Sh) and the fluidization conditions (typically represented by dimensionless numbers Re , Sc and ϵ). Most of these correlations are obtained in conventional fluidized beds.

In a conventional two-phase (liquid-solid) fluidized bed, a common way to enhance mass transfer coefficient (for a particular type and size of particles) is to increase the liquid velocity u_l . However, an increase in liquid velocity results in increased bed porosity ϵ_l . This means that the fluid interstitial velocity ($u_{l,int} = \frac{u_l}{\epsilon_l}$), which is the relative velocity between the fluid and the fluidizing particles, may not change at all. Hence, the mass transfer coefficient, which depends primarily on $u_{l,int}$, will stay the same or even decrease.

It is well known, however, that, in a three-phase fluidized bed, higher liquid-solid mass transfer coefficient can be attained by increasing the gas flow. The most promising correlations found in literature are based on the phenomenological theory of isotropic turbulence proposed by Kolmogoroff (Hinze, 1975). The energy dissipation model proposes that the mass transfer is directly related to the turbulent intensity of fluid eddies in a very small volume around the particle, and that the properties of these eddies

Table 3-1 Liquid-Solid Mass Transfer Correlations

Reference	Expt Technique	Fluid	Particles	Bed	ε range	Re range	Correlation
Fan et al.(1960)	Dissolution	Water	Granules .7-2.1mm	Fixed and fluidized bed (2 phase)	0.65-0.9	1020-1520	$Sh = 2 + 1.51(Re(1 - \varepsilon))^{0.5} Sc^{1/3}$
Couderc et al.(1971)	Dissolution	Water	Benzoic acid spheres 4.9-8.2mm	Fluidized bed (2phase)	0.5-0.75	100-300	$Sh = \frac{0.0054}{\varepsilon^2} Re Sc^{1/3}$
Damrong-lerio et al.(1973)	Dissolution	Water	Benzoic acid spheres 4.6-8.2mm	Fluidized bed (2phase)	0.6-0.95	1300-1600	$Sh = 0.763\varepsilon^{-1.2} Re^{0.556} (\varepsilon < 0.815)$ $Sh = 0.268\varepsilon^{-2.4} Re^{0.669} (\varepsilon > 0.815)$
Laguerie (1976)	Dissolution	Saturated aqueous soln.	Citric acid crystal	Fluidized bed (2phase)	0.65-0.95	0.12-1.2	$Sh = 0.36 Re^{0.5} Sc^{0.333} \varepsilon^{-1.8}$
Nanda et al. (1975)	Dissolution	Water	Benzoic acid	Fluidized bed (2phase)	0.4-0.95	6.5-900	$J_d \varepsilon = .0213 f$ $Re'' < 1000$
Upadhya and Tripathi (1975)	Dissolution	Water	Benzoic acid cylinders and pellets	Fluidized bed (2phase)	0.27-0.91	572-1350	$J_d = 3.8155 Re''^{-0.7313} (Re'' < 20)$ $J_d = 1.6218 Re''^{-0.477} (Re'' > 20)$
Ganho et al. (1975)	Adsorption	Phenol in aqueous soln.	Activated carbon	Fluidized bed (2phase)	0.59-0.83	6-22	$J_d = 2.55 Re^{-0.537}$

Table 3-1 (continued)

Reference	Expt. Technique	Fluid	Particles	Bed	Re range	Correlation
Kikuchi et al.(1983)				fluidized bed (2 phase and 3phase)	$0 < (e^{1/3} d_p^{4/3} / \nu_l) < 10^3$	$Sh = 2 + 0.51(e^{1/3} d_p^{4/3} / \nu_l)^{0.60} Sc^{1/3}$ where $e = [(U_g + U_l)(\epsilon_s \rho_s + \epsilon_l \rho_l + \epsilon_g \rho_g) - U_l \rho_l - U_g \rho_g] g / \epsilon_l \rho_l$
Arters and Fan (1986)	Dissolution	Water and Air	Benzoic acid particles	fluidized bed (2 and 3phase)	$17.4 < Re_l < 253$ $0.00 < Re_g < 98.0$ $22.3 < Ga < 562$ $1960 < Sc < 3550$	$Sh = 0.228(1 + 0.826 Re_g^{0.623}) \Phi^{1.35}$ $Ga^{0.323} Mv^{0.300} Sc^{0.400}$
Fukuma et al.(1988)	Ion exchange	Electrolyte solution and Nitrogen gas	Ferricyanide ion spheres 3.1-4.8mm	fixed and fluidized bed (2 and 3 phase)	$1 < e^{1/3} d_p^{4/3} / \nu_l < 10^4$	$Sh = 2 + 0.51(e^{1/3} d_p^{4/3} / \nu_l)^{0.60} Sc^{1/3}$ $e = (\Delta P_d / d_p) U_l / \epsilon_l \rho_l + U_g g + (\Delta P_w / h) U_l / (\epsilon_l \rho_l)$
Al-Muhlim and Jovanovic (1995)	Adsorption	Methylene blue in aqueous soln.	ferromagnetic particles	MSFB (2 phase)		$Sh = \frac{0.0365}{\epsilon^2} Re Sc^{0.33}$ $\epsilon = \epsilon_{ms} + (\epsilon_{ff} - \epsilon_{ms}) \exp(-(1 - \epsilon)(\alpha H + \beta) \frac{H}{H_{ms}})$

may be determined by the rate of energy dissipated per unit mass of fluid in the bed. Several correlations have arisen from this concept of energy dissipation in three-phase fluidized beds. Kawase et al. (1987) and Fukuma et al. (1988) applied the concept of energy dissipation to three-phase fluidized bed systems and found the following correlations, respectively.

$$Sh = 0.162 (E d_p^4 / \nu_l^3)^{1/4} Sc^{1/3} \quad \text{Kawase et al. (1987)} \quad (3-1)$$

$$Sh = 2 + 0.51 (E d_p^4 / \nu_l^3)^{0.20} Sc^{1/3} \quad \text{Fukuma et al. (1988)} \quad (3-2)$$

where it is considered valid over the range

$$1 < (E^{1/3} d_p^{4/3} / \nu_l) < 10^4$$

For both equations, E is the rate of energy dissipated per unit mass of fluid in the bed, which is defined as

$$E = \frac{g \{ (u_l + u_g) (\varepsilon_s \rho_p + \varepsilon_l \rho_l) - u_l \rho_l \}}{\varepsilon_l \rho_l} \quad (3-3)$$

In a three-phase Magnetically Stabilized Fluidized Bed (MSFB), an additional phenomena can be created by applying a magnetic field on ferromagnetic particles. Therefore, the mass transfer coefficient can be enhanced not only by the increase of the gas phase flow rate but by the positive influence of the magnetic field. Al-Mulhim (1995) had experimentally shown, in a two-phase MSFB with uniform magnetic field, that the mass transfer coefficient can be enhanced with the application of stronger uniform magnetic field. In his paper, he claimed the magnetic field magnetizes the ferromagnetic particles and they are attracted to each other, resulting in a change of the

bed structure, i.e. the decrease of the liquid porosity. He also claimed the decrease of the liquid porosity will eventually result in the enhancement of the mass transfer coefficient because, even though the liquid velocity stays the same, the liquid interstitial velocity ($u_{l,int} = \frac{u_l}{\epsilon_l}$) increases. Villers (1998) proposed the new concept of 'particle virtual diameter' trying to explain the reason why the liquid porosity decreases when the uniform magnetic field is applied. He suggested the small clusters of particles formed are seen by the fluid as a single particle having a larger diameter. Since the fluid flow rate is not changed, the drag force exerted on particle clusters is then not sufficient to support the weight of these virtual particles. Therefore, the height of the bed must decrease to a point at which a new equilibrium of forces is reached. The decrease in bed height reduces the liquid porosity of the bed and increases the interstitial liquid velocity, which will then increase the drag force to balance the increase in particle size. Figure 3-1 shows the forces exerted on the uniform and the non-uniform magnetic field.

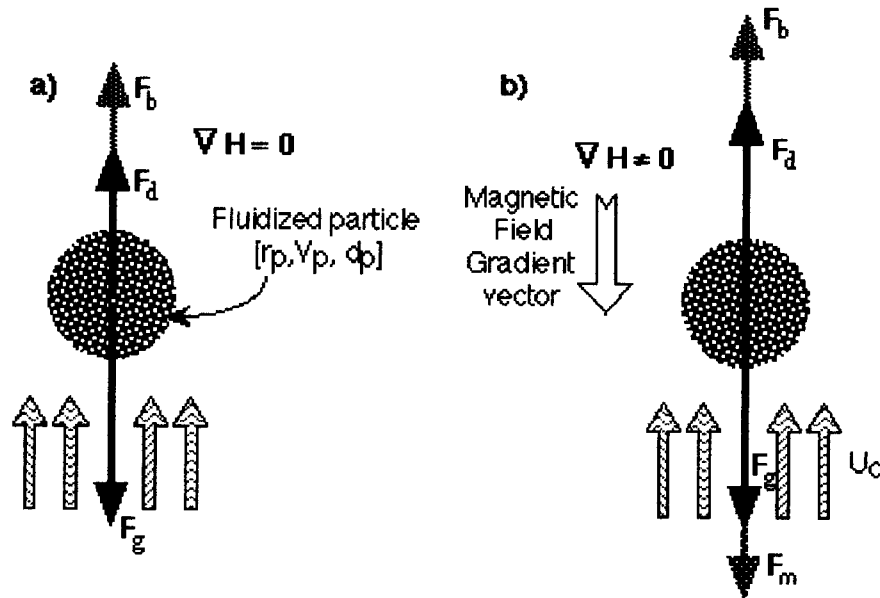


Figure 3-1 Balance of Forces a) when uniform magnetic field is applied, and b) when there is magnetic field gradient

The following is the liquid-solid mass transfer correlation in two-phase MSFB proposed by Al-Mulhim (1995).

$$Sh = \frac{0.036}{\varepsilon^2} Re Sc^{1/3} \quad (3-4)$$

where

$$\varepsilon = \varepsilon_{ms} + (\varepsilon_{ff} - \varepsilon_{ms}) \exp(-(1 - \varepsilon)(\alpha H + \beta) \frac{H}{H_{ms}}) \quad (3-5)$$

Consequently, in 3-phase MSFB, we can expect, in some range, the combining effect of gas agitation and magnetic field, and that it will enhance the mass transfer between particles and the liquid phase even more than ordinary 3-phase fluidized bed or 2-phase MSFB. This is illustrated in Figure 3-2.

3.2 Mathematical Model for the Adsorption in Three-phase MSFB

A mathematical model is used to evaluate mass transfer coefficient in three-phase MSFB. The model and the experimental system is schematically represented by Figure 3-3:

System boundary (1) represents the part of the system (including part of the fluidization column, overflow box, connecting pipes, pump, rotameter, etc.) where only the adsorbate solution is present (no fluidizing particles). It is assumed that in this volume the fluid is very well mixed and hence the adsorbate concentration C is uniform. System boundary (2) is the part of the system where the fluidizing particles are in contact with the adsorbate and where the actual mass transfer is taking place.

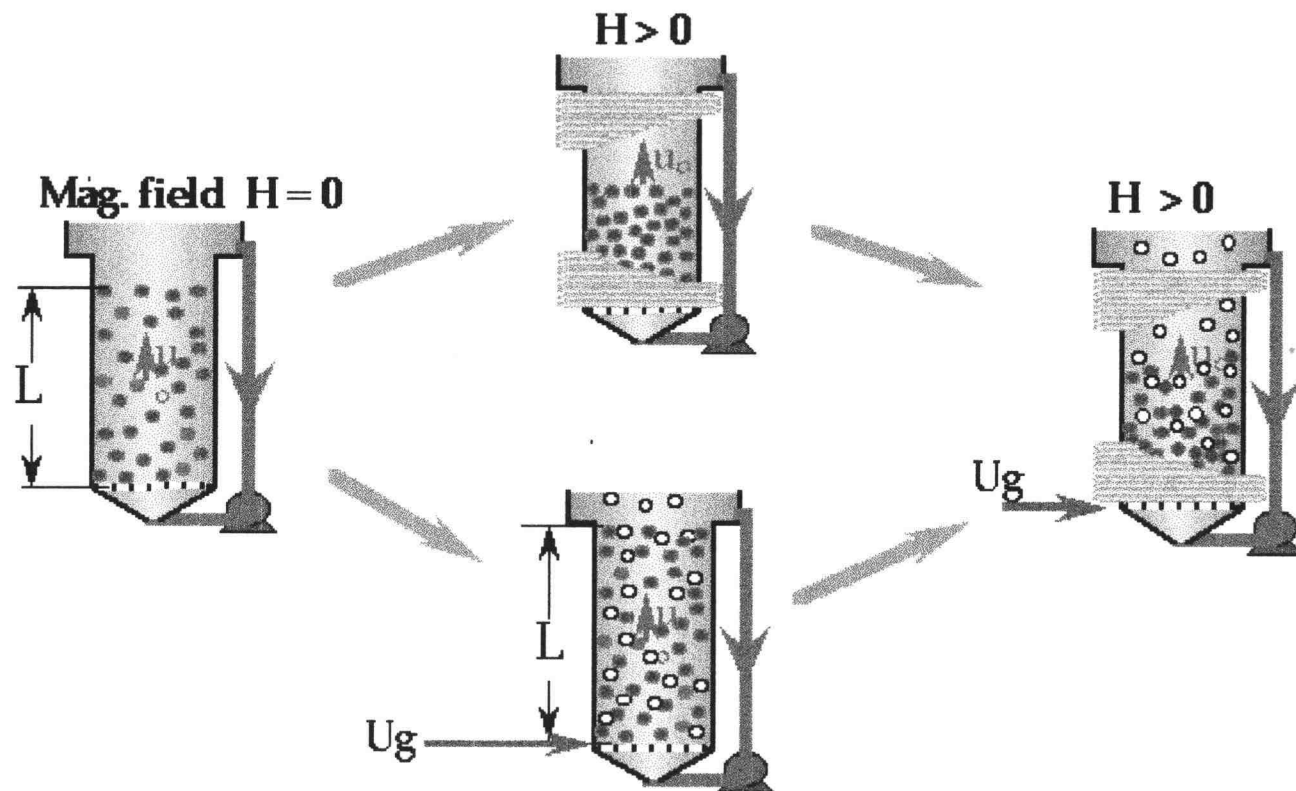


Figure 3-2 Combining Effect of Gas Agitation and Magnetic Field

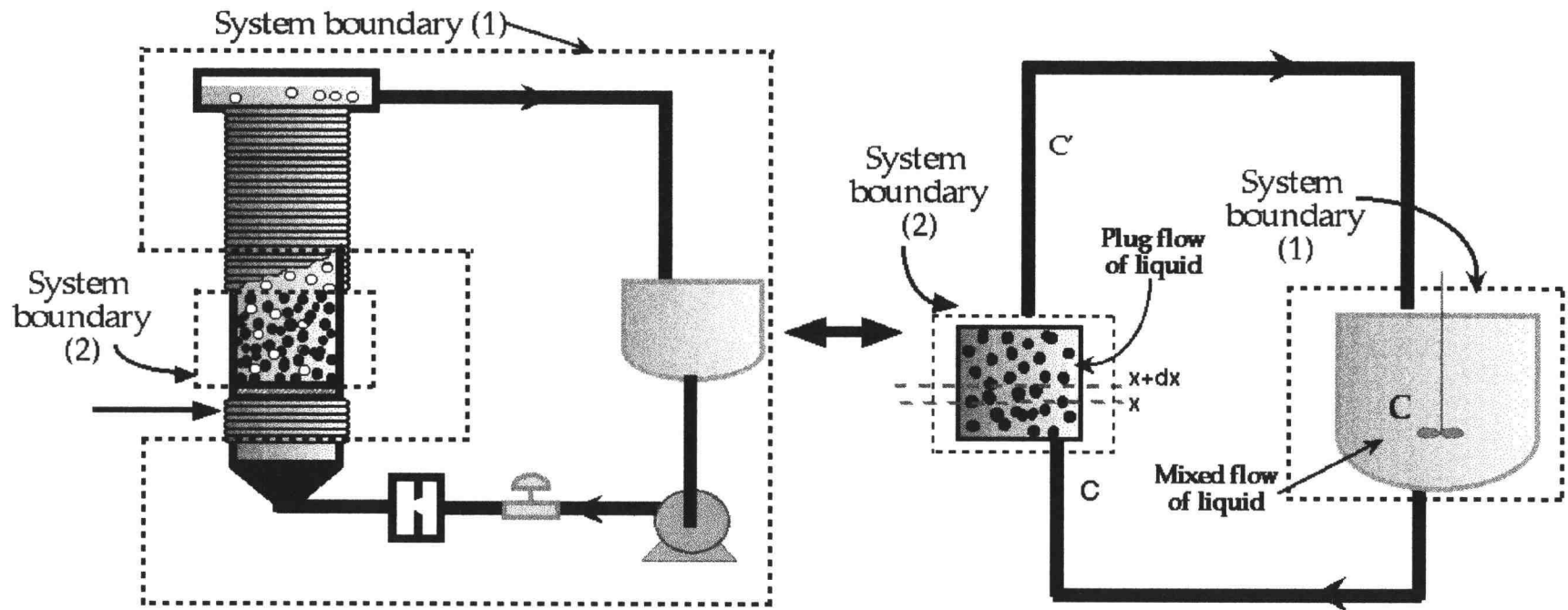


Figure 3-3 The Experimental System and the Model

3.2.1 Assumptions

1. The fluid is very well mixed in system boundary (1). Therefore we can assume that the adsorbate concentration within system boundary (1), C , is uniform. This is an obvious assumption because no adsorption is taking place there and the recirculating pump is a part of this system.
2. The flow of fluid through the fluidized bed is a plug flow.
3. The following three steps is the characteristics of the MB transport from the liquid to the particles,

- 1) mass transfer of MB from bulk liquid to particle surface
- 2) intraparticle diffusion
- 3) adsorption at an interior site

and step 3 is much faster with respect to the first two steps. For this reason the MB adsorption isotherm is very much important for all considerations and calculations.

We also need an assumption that the adsorption isotherm is linear in a dilute range of MB concentrations. This assumption is proposed by several researchers, McKay et al. (1985) and Tang (1990) as well as Al-Mulhim (1995). To verify this assumption, the adsorption isotherm is established for this study (see Chapter 4 for details). A linear isotherm is obtained and represented by the following equation:

$$N = K_e C_s \quad [\text{g of MB/g particles}]$$

4. C_s is constant during one pass of the fluid through the fluidized bed. This assumption makes C_s only a function of time.

5. It is assumed there is no contact between the gas phase and the particles although gas agitation has a great effect on the mass transfer. In this case, a' is constant for all different magnetic field and gas flow rate, which is not true, especially when relatively stronger magnetic field and higher gas flow rate are applied. However, in the experimental range, since the particle size is approximately the same order of magnitude as the bubble size (3 mm particle size and about 4.5 mm bubble size are used) and the volume occupied by the gas is at most 4% (see Figure 5-1), it is assumed there are enough room for bubble to pass through between the particles with negligible contact time. This assumption is convincing since the bubbles don't seem to break itself when they are rising. There will be more discussion about this later in Chapter 5 and 6.

6. Particles are not moving, of the same size and all spherical.

7. $\rho_p, \varepsilon_p, D_e, m_s, k$ are constant

- For the analytical solution, there should be further assumptions.

8. The adsorbate concentration at the inlet of the fluidized bed, C^* , is not changing substantially while the fluid passes through the fluidized bed (quasi-steady state assumption). This assumption was also used by other investigators such as Tang (1990), Al-Mulhim (1995).

9. The intraparticle diffusion resistance is negligible. Since most parts of the particles are water, particles' internal volume is readily accessible to the adsorbate. Also, as mentioned later in Chapter 5, mass transfer calculations are based on the initial adsorption data, where diffusion resistance plays very minor role. Several investigators, such as Furusawa and Smith (1973), McKay (1983), Silem et al. (1993) and Al-Mulhim (1995) neglected the intraparticle diffusion in the development of their model.

3.2.2 Derivation of the Model

1) Material Balance of Methylene Blue for the system boundary (1)

$$FC' - FC = V \frac{dC}{dt} \Rightarrow F(C' - C) = V \frac{dC}{dt} \quad (3-6)$$

with initial condition 1-1 $C = C_0$ (at $t=0$)

2) Material Balance of Methylene Blue for the system boundary (2)

$$(FC^*)_x - (FC^*)_{x+\Delta x} - k(C^* - C_s)a = \varepsilon_l A \Delta x \frac{\partial C^*}{\partial t}$$

where

$$a = a' A \Delta x .$$

Therefore,

$$-F \frac{\partial C^*}{\partial x} - ka' A (C^* - C_s) = \varepsilon_l A \frac{\partial C^*}{\partial t} \quad (3-7)$$

with boundary conditions 2-1 $C^*(x, t) = C(t)$ (at $x=0$)

2-2 $C^* = C'(t)$ (at $x=L$)

and initial condition 2-1 $C^* = C_0$ (at $t=0$ and at any x)

However, with the further assumption 8, $\frac{\partial C^*}{\partial t} = 0$ and equation (3-7) can be

$$F \frac{dC^*}{C^* - C_s} = -ka' A dx \quad (3-8)$$

3) Material Balance of Methylene Blue for the differential element in a particle

$$\begin{aligned}
 & D_e (4\pi r^2) \frac{\partial C_r}{\partial r} \Big|_{r+\Delta r} \Delta t - D_e (4\pi r^2) \frac{\partial C_r}{\partial r} \Big|_r \Delta t \\
 & - \mathfrak{R}(C_r) 4\pi r^2 \Delta r \varepsilon_p \Delta t \\
 & = C_r (4\pi r^2) \varepsilon_p \Delta r \Big|_{t+\Delta t} - C_r (4\pi r^2) \varepsilon_p \Delta r \Big|_t
 \end{aligned}$$

Dividing by $\Delta r \Delta t$, taking the limit as $\Delta r \rightarrow 0$ and $\Delta t \rightarrow 0$ and arranging it leads to

$$\frac{D_e}{\varepsilon_p} \frac{\partial}{\partial r} \left(r^2 \frac{\partial C_r}{\partial r} \right) - \mathfrak{R}(C_r) r^2 = r^2 \frac{\partial C_r}{\partial t}$$

and

$$D \left(\frac{\partial^2 C_r}{\partial r^2} + \frac{2}{r} \frac{\partial C_r}{\partial r} \right) - \mathfrak{R}(C_r) = \frac{\partial C_r}{\partial t} \quad (3-9)$$

where $\mathfrak{R}(C_r)$ is the generation rate of MB ($= m \frac{\partial N}{\partial t}$)

$$\text{and } \frac{D_e}{\varepsilon_p} = D$$

with boundary conditions 3-1. $D\left(\frac{\partial C_r}{\partial r}\right)_s = k(C^* - C_s)$ (at $r = R$)

$$3-2. \left(\frac{\partial C_r}{\partial r}\right) = 0 \quad (\text{at } r = 0)$$

and an initial condition 3-1 $C_r = 0$ (at $t = 0$ for $0 \leq r \leq R$)

However, the further assumption 9 makes equation (3-9) unnecessary.

3.2.3 Solving the Model Equation

There are two ways of solving the mathematical equation. The numerical method using FORTRAN 77 programming (Appendix E) is tried with equations (3-6), (3-7) and (3-9) along with the boundary conditions and initial conditions. However, the resolution problem came up and we failed to find the right range of diffusion coefficient (see Appendix F). Thus, instead, analytical method is tried with some further assumptions 8 and 9. The analytical solution of the mathematical model is shown in Appendix G.

The useful form of the final solution from Appendix G is represented by the following equation:

$$\ln\left\{\frac{C(1+mK_e)-C_0}{C_0(1+mK_e)-C_0}\right\} = \frac{1+mK_e}{mK_e} \frac{F}{V} (e^{-\alpha t} - 1)t \quad (3-10)$$

where

$$\alpha = \frac{a' AL}{F} \quad (3-11)$$

CHAPTER 4 EXPERIMENTAL MEASUREMENTS

4.1 Adsorption Isotherm

As explained in section 3.2, a linear relationship is assumed between equilibrium concentration of methylene blue (MB) in the solution and the amount of MB adsorbed on the particles. To verify this assumption, the adsorption isotherm for MB and the fluidizing particles is determined by measuring the steady state MB concentration C_{ss} for different initial concentrations C_0 . In every run, the same amount of particles is used. A plot of C_{ss} versus N is established, where N is the concentration of MB adsorbed on the fluidizing particles and it is evaluated from the equation:

$$N = \frac{C_0 - C_{ss}}{m} \quad (4-1)$$

where m is the mass of particles used per unit volume of fluid.

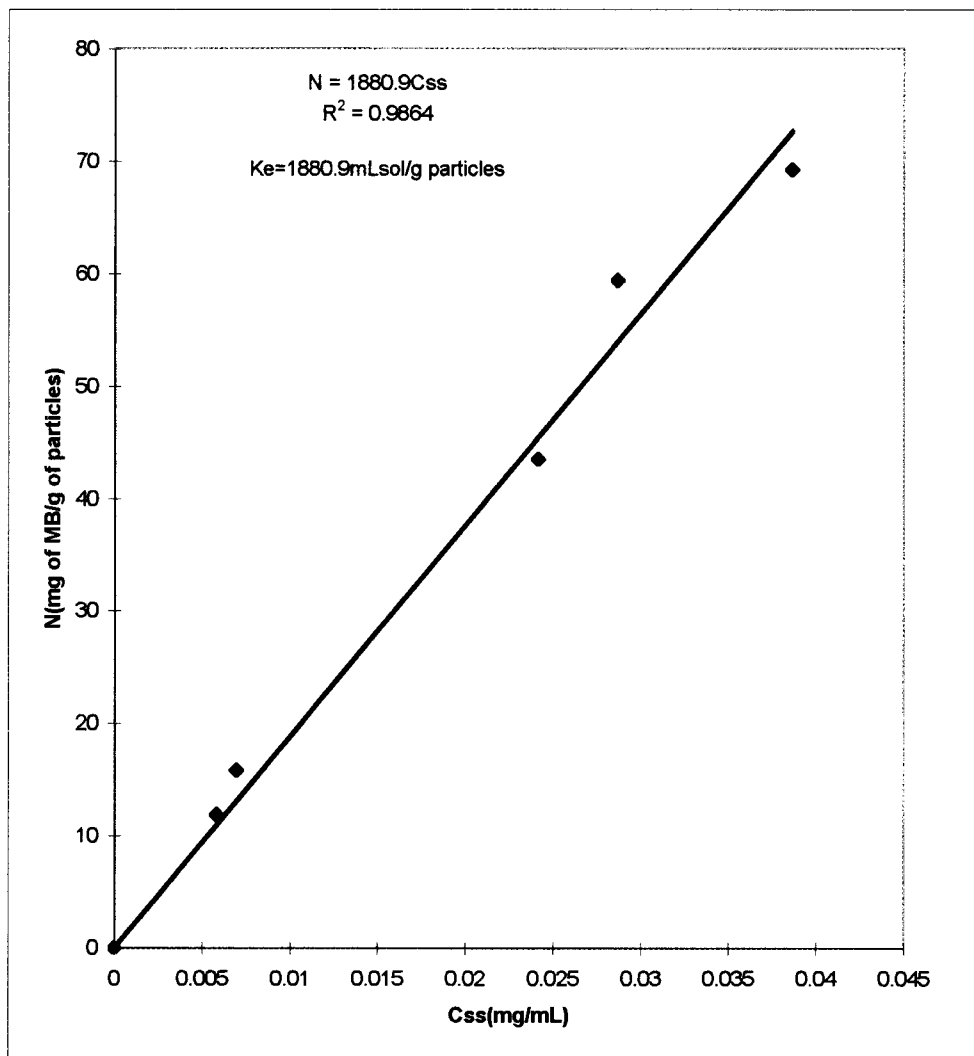
Table 4-1 and Figure 4-1 report the adsorption isotherm data at $25^\circ C$ at this low concentration range. The adsorption isotherm shows a noticeable linear relationship. The data are linearly fitted and the following relationship is obtained:

$$N = K_e C_{ss} \quad (4-2)$$

where K_e is the adsorption equilibrium constant and its value is the slope of the fitted straight line.

Table 4-1 : Adsorption Isotherm Data

initial concentration C_0 [mg/ml]	N [mg of MB/g of particles]	steady state MB conc. C_{ss} [mg/ml]
0.0	0.0	0.0
0.6	11.88286	0.005857
0.8	15.86082	0.006959
2.2	43.517	0.02415
3.0	59.42594	0.028703
3.5	69.22694	0.038653

Figure 4-1 Adsorption Isotherm Plot

4.2 The Height and Porosity of the Bed

To obtain mass transfer coefficient and to find an appropriate correlation, gas and liquid porosities have to be determined in any forms.

The pressure drop through the bed is strongly related to the individual phase holdups in the bed. In the fluidized bed with low solids entrainment rates, the volume fraction of the solids, or solids holdup, can be expressed in terms of the total mass of solids (W_s), the solid density (ρ_p), the cross section of the column A, and the effective bed height (L) as

$$\varepsilon_s = 1 - \varepsilon = \frac{W_s}{\rho_p AL} \quad (4-3)$$

On the other hand, at steady state conditions with low or moderate liquid and gas velocities, the total vertical pressure gradient (static pressure gradient) can be

$$-\frac{dP}{dx} = (\varepsilon_s \rho_p + \varepsilon_l \rho_l + \varepsilon_g \rho_g)g \quad (4-4)$$

In this equation the frictional drag on the column wall and the acceleration terms for the gas and liquid flows are neglected. Since the contribution of the gas phase is usually negligible compared to the other terms, equation (4-4) can be simplified to

$$-\frac{dP}{dx} = (\varepsilon_s \rho_p + \varepsilon_l \rho_l)g \quad (4-5)$$

This equation permits evaluation of individual phase holdups from the pressure gradient. ε_s can be directly obtained from equation (4-3) with the measured

effective bed height L . And although it is not easy to decide the effective bed height L , with the concept of the dynamic pressure gradient for the liquid, it can be measured (See Figure 4-2 for determining L).

When liquid is the continuous phase, the dynamic pressure gradient for the liquid ($-dP_d/dx$), defined as the total pressure gradient corrected for the hydrostatic head of the liquid is

$$-\frac{dP_d}{dx} = \left(-\frac{dP}{dx}\right) - \rho_l g \quad (4-6)$$

and it can be measured directly by the head of the liquid phase. (See chapter 2 for details)

In Appendix H, the dynamic pressure at each port for different gas flow rates and different magnetic fields are attached.

Fig 4-3 shows a typical example of axial dynamic pressure variation for a three-phase fluidized bed. The dynamic pressure distribution shows linear behavior in both the bulk fluidized bed region and the freeboard region above the bed. Both the dynamic pressure and the pressure gradient decrease with increasing gas velocity because of increased gas holdup. The location of the expanded bed height L can be determined from the intersection of the linear pressure profiles in the bulk fluidized bed and freeboard regions. (Fan et al.) Once $-dP_d/dx$ and ε_s are determined, by combining equation (4-5) and (4-6), ε_l and ε_g can be obtained too. The bed heights and calculated porosities for different gas flow rates and magnetic fields are tabulated in Table 4-2. The slight error (for example, (-) gas porosity) could have been caused by the uncertainty in determination of the effective bed height L .

Figure 4-2 Determination of the Bed Height L

($U_l = 5 \text{ cm/s}$, $U_g = 0.27 \text{ cm/s}$ and $H = 4.28 \text{ kA/m}$)

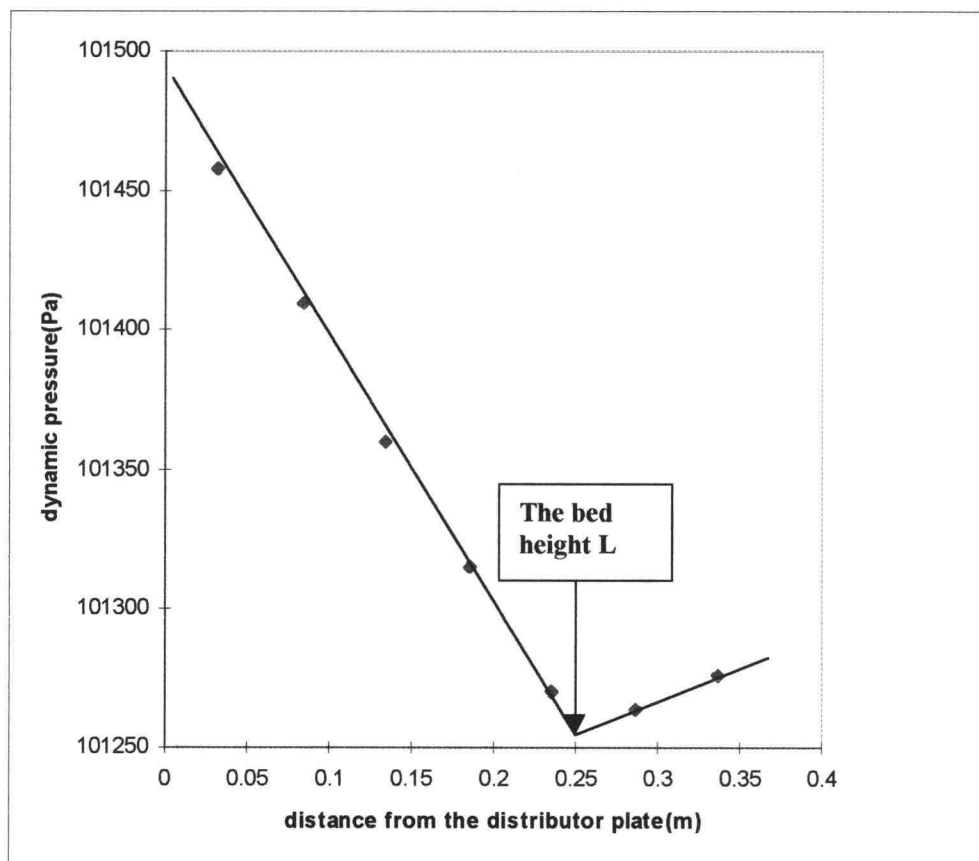


Figure 4-3 Axial Dynamic Pressure at $H=4.28\text{kA/m}$ and at Liquid Velocity 5 cm/s

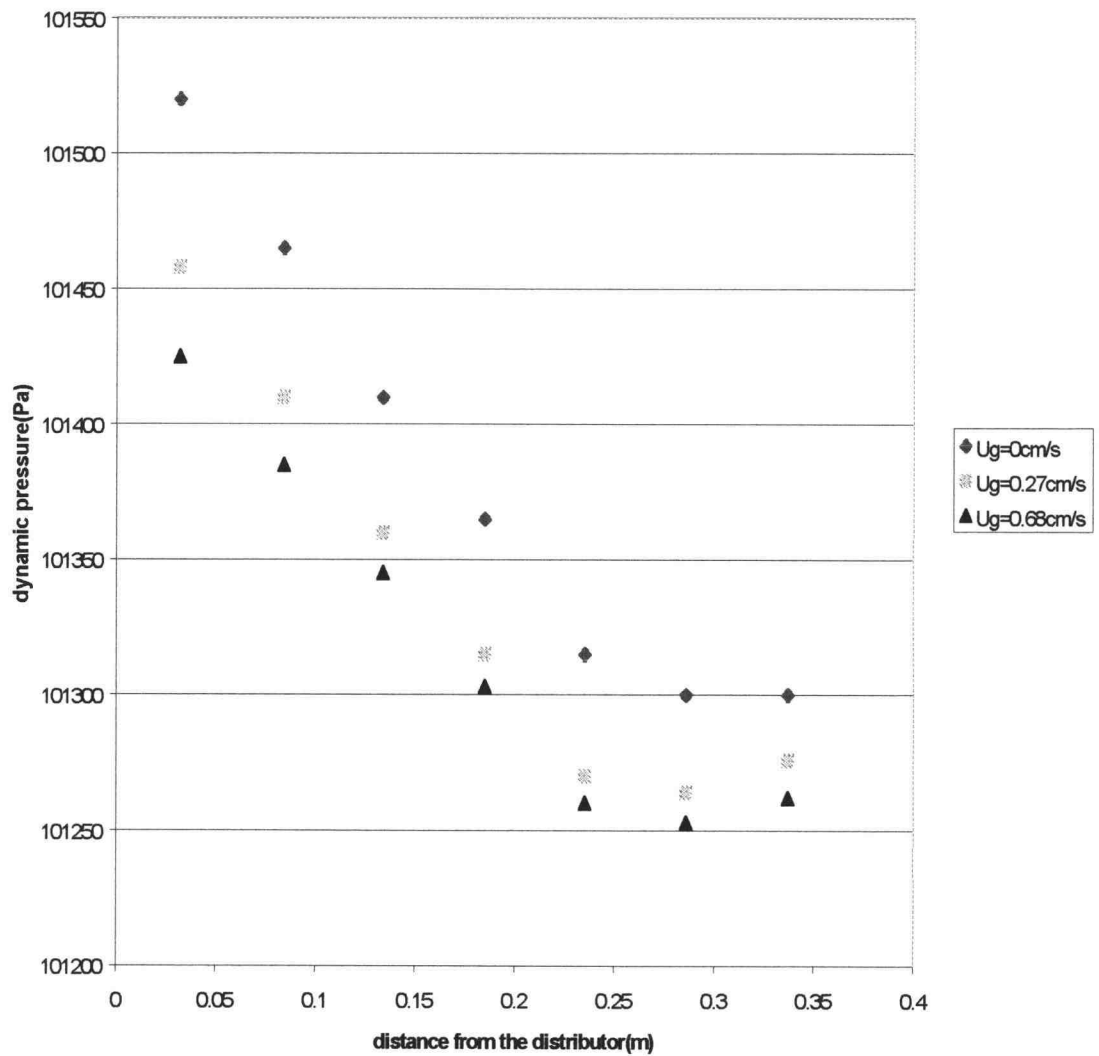


Table 4-2 Bed heights and Porosities of Each Run (at Liquid Flow Rate = 5 cm/s)

magn. field (kA/m)	air flow (cm/s)	$-\frac{dP_a}{dz}$ (Pa/m)	L(cm)	ε	ε_l	ε_g
0	0	966.51	27.42	0.7986	0.79960	-0.00098
0	0.27	788.92	27.61	0.8001	0.7836	0.01650
0	0.68	651.11	28.10	0.8037	0.7747	0.02900
4.28	0	1006	24.85	0.7771	0.7727	0.00436
4.28	0.27	929	24.91	0.7776	0.7656	0.01199
4.28	0.68	812.53	25.18	0.7801	0.7573	0.02281
7.71	0	1178.7	21.89	0.7460	0.7457	0.00027
7.71	0.68	931.32	22.02	0.7475	0.7227	0.02485
7.71	0.967	848.84	22.84	0.7568	0.7276	0.02921
11.2	0	1286.7	19.90	0.7198	0.7192	0.00062
11.2	0.27	1119.7	20.45	0.7276	0.7133	0.00143
11.2	0.68	1011.9	20.55	0.7290	0.7043	0.02470
11.2	1.172	785.81	21.84	0.7454	0.7047	0.04063

4.3 Measurements of the MB Concentration in Three-phase MSFB

Original concentration data using the MB adsorption on the fluidizing particles are reported in Appendix I. Liquid superficial velocity is fixed with different gas flow rate and different magnetic field intensities. In all experiments, same amount of the fluidizing particles and fluid volume are used.

CHAPTER 5

EXPERIMENTAL RESULTS AND DISCUSSION

For the correlation between the mass transfer coefficient and the operating conditions to be derived, we need reliable information about how the magnetic field affects the porosities. That is to say, we need a correlation between porosities and magnetic field first.

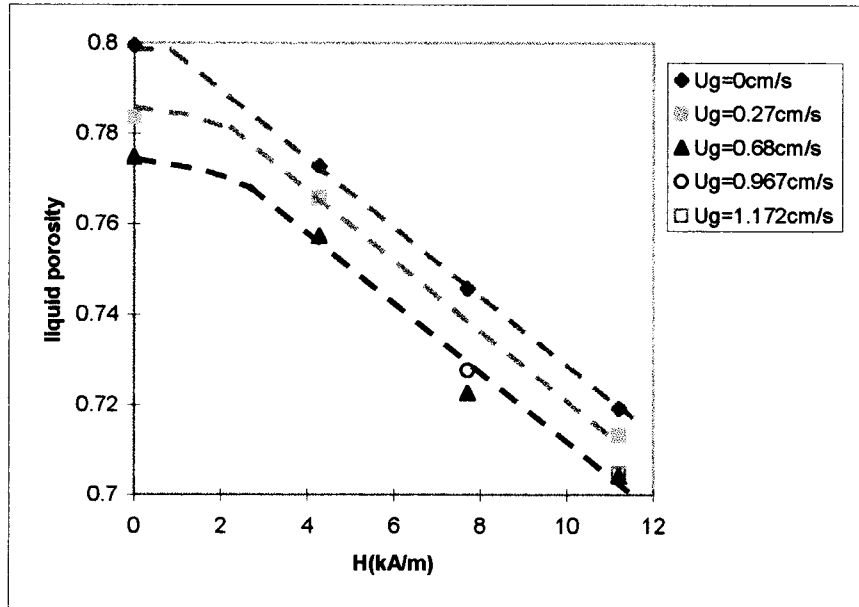
5-1 The Average Porosity of the Liquid and the Gas Phase

Figure 5-1 shows the average porosity of each of the phases as a function of the magnetic field for different gas flow rates. From this Figure, within the range of experimental conditions, we can conclude that:

- 1- For a given gas velocity, the liquid porosity decreases when magnetic field intensity increases (Figure 5-1 (a)).
- 2- For a given gas flow rate, the gas porosity ε_g is not affected by the magnetic field (Figure 5-1 (b)).

Even though there is no correlation between the porosity and the magnetic field found in the literature for a three-phase MSFB, the correlation of the liquid porosity with the magnetic field in liquid-solid two-phase MSFB was studied by several investigators including Siegel (1987), Kwauk (1992), Jovanovic et al. (1993), Honorez (1994) and Villers (1998). With the conclusion made above (the gas porosity is not affected by the magnetic field changes at the constant gas and liquid flow rate), the equations derived for the two phase (liquid-solid) MSFB could be extended to the three-phase MSFB. The lines in Figure 5-1 (a) and (b) are drawn under this conclusion.

a)



b)

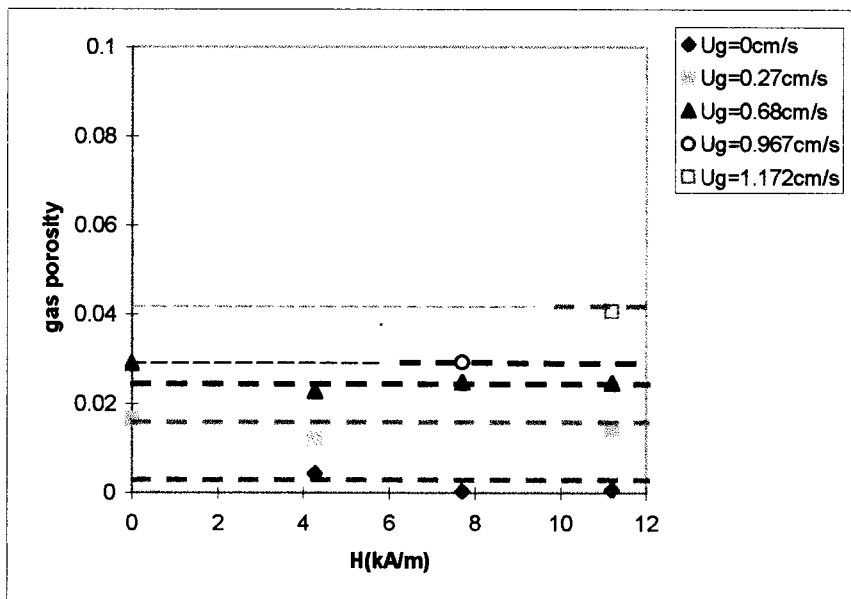


Figure 5-1 The Average Porosities as a Function of Magnetic Field Intensity for Different Gas Velocities

Kwauk (1992) and Honorez (1994) presented similar plots as Figure 5-1 (a) and suggested the following equations.

$$\varepsilon_l = \varepsilon_{l,ms} + (\varepsilon_{l,ff} - \varepsilon_{l,ms}) \exp\left[-\frac{H}{H_0}\right]^{S_k} \quad \text{Kwauk (1992)} \quad (5-1)$$

where S_k is the slope of the straight line and H_0 is the intercept of the $\varepsilon - H$ log-log graph.

$$\varepsilon_l = \varepsilon_{l,ms} + (\varepsilon_{l,ff} - \varepsilon_{l,ms}) \exp\left(-(1 - \varepsilon_l)(\alpha H + \beta) \frac{H}{H_{ms}}\right) \quad \text{Honorez (1994)} \quad (5-2)$$

where $\varepsilon_{l,ff}$ is the liquid porosity of an ordinary fluidized bed (at $H=0$), $\varepsilon_{l,ms}$ and H_{ms} are the liquid porosity and magnetic field intensity at the transition between the partially stabilized and stabilized regime. This characteristic transition is attained when the liquid porosity reaches the minimum value and does not decrease anymore with the increase of the magnetic field intensity, i.e., the ferromagnetic particles are “frozen”. In a three-phase MSFB, $\varepsilon_{l,ff}$, $\varepsilon_{l,ms}$ and H_{ms} are functions of the gas and liquid flow rate. The transition from the partially stabilized regime to the stabilized regime also depends strongly on the construction and design of the distributor plate (Siegell, 1987). Sometimes it is difficult to distinguish between these two regimes. The detailed description of this and other fluidization regimes are given elsewhere, Rosensweig (1981), Siegell (1987,1988), Casal and Arnaldos (1991) and Honorez (1994).

We can now conclude that the magnetic field intensity has a significant effect on the liquid porosity. This is the result that we expected and which we believe will have a substantial influence on the enhancement of the liquid-solid mass transfer coefficient.

5.2 Mass Transfer Coefficient Calculation

The following parameters are kept constant in all of the experiments conducted in this study:

$$V_L = 15000[\text{mL}]$$

$$M=170.73 [\text{g}]$$

$$\varepsilon_{l,0}=0.417$$

$$d_p = 0.3 [\text{cm}]$$

$$L_0 = 9.8 [\text{cm}]$$

$$F=Au_l = 104.15 [cm^3 / s]$$

The calculation of the liquid-solid mass transfer coefficient is based on the outer surface of particles which is calculated as:

$$a' = \frac{(1 - (\varepsilon_g + \varepsilon_l))A_p}{V_p} = \frac{6(1 - (\varepsilon_g + \varepsilon_l))}{d_p} \left[\frac{cm^2 \text{ particle surface}}{cm^3 \text{ of column}} \right] \quad (5-3)$$

Furthermore, equation (3-10) can be written as:

$$\ln \frac{(C/C_0)(1 + mK_e) - 1}{mK_e} = \frac{1 + mK_e}{mK_e} \frac{F}{V} (e^{-ak} - 1)t \quad (5-4)$$

Hence, a plot of $\ln \frac{(C/C_0)(1 + mK_e) - 1}{mK_e}$ versus time, t, should give us a straight line

with a slope, S.

$$S = \frac{1 + mK_e}{mK_e} \frac{F}{V} (e^{-ak} - 1) \quad [1/s] \quad (5-5)$$

However, as shown in Figure 5-2, we see that the plot shows a clear straight line only at the beginning of the adsorption (approximately up to 600 seconds in Figure 5-2) and then the concentration curve starts to deviate from linearity. Equation (5-4) is developed under the assumption that the mass transfer resistance due to diffusion within the particles is negligible. Obviously, this is not the case and we have to be very careful how to measure the slope of equation (5-4). Consequently, the slope is taken at the beginning of the adsorption data where the plot is clearly linear and the assumption of neglecting diffusion resistance is reasonably valid, simply because it does not have predominant influence at the very beginning of the experiment.

Substituting the values of the slopes into equation (5-5), we can obtain

$$S = \frac{1 + 1880.9m}{1880.9m} \frac{104.15}{V} (e^{-ak} - 1) \Rightarrow \quad (5-6)$$

$$k = -\frac{1}{\alpha} \ln\left(\frac{1880.9mSV}{104.15(1 + 1880.9m)} + 1\right) \quad [\text{cm/s}] \quad (5-7)$$

where

$$\begin{aligned} m &= M/AL \varepsilon_l \\ &= 170.73 / (20.83 \times L_0 (1 - \varepsilon_{l,0} - \varepsilon_{g,0}) / (1 - \varepsilon_l - \varepsilon_g) \times \varepsilon_l) \\ &= 1.43 \frac{1 - \varepsilon_l - \varepsilon_g}{\varepsilon_l} \quad [\text{g particles/mL solution}] \end{aligned} \quad (5-8)$$

$$\begin{aligned} V &= V_L - AL \varepsilon_l = V_L - A \frac{L_0 (1 - \varepsilon_{l,0} - \varepsilon_{g,0})}{1 - \varepsilon_l - \varepsilon_g} \varepsilon_l \\ &= 15000 - \frac{119.01 \varepsilon_l}{(1 - \varepsilon_l - \varepsilon_g)} \quad [\text{mL}] \end{aligned} \quad (5-9)$$

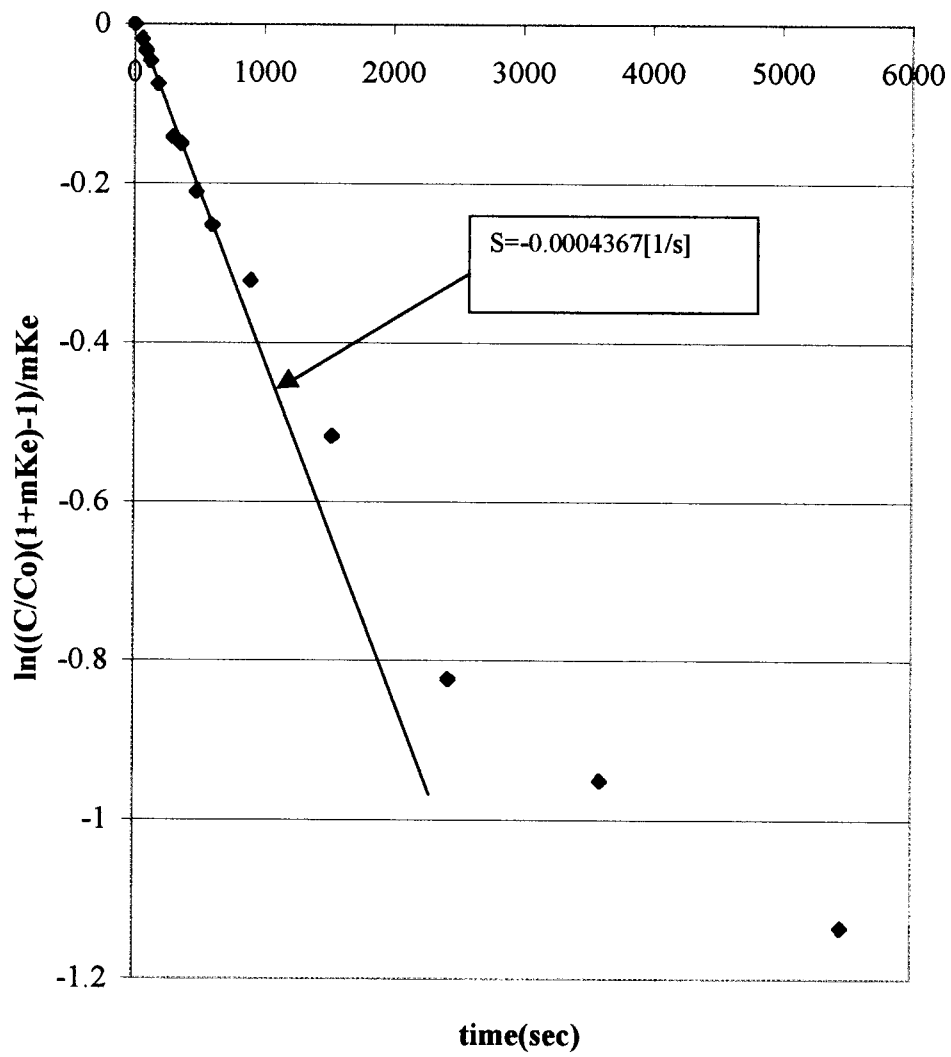


Figure 5-2 Determination of the Initial Slope S

$(U_l = 5\text{ cm/s}, U_g = 0\text{ cm/s}, H = 4.28\text{ kA/m})$

$$\alpha = \frac{a' AL}{F} = \frac{6(1 - \varepsilon_l - \varepsilon_g)}{d_p} \frac{AL}{Au_l} = \frac{6(1 - \varepsilon_{l,0})L_0}{d_p u_l} = 22.85 \quad [\text{s/cm}] \quad (3-11)$$

From the above equations (5-7), (5-8), (5-9) and (3-11), mass transfer coefficient k can be evaluated.

Table 5-1 summarizes the values of the measured mass transfer coefficients for different fluid velocities and different magnetic field intensities. The values are plotted as a function of magnetic field intensities for different gas velocities on Figure 5-3 and as a function of gas velocities for different magnetic field intensities on Figure 5-4.

**Table 5-1 Measured k Values
for Different Gas Velocities and Different Magnetic Field Intensities.**

Run #	Magnetic Field (kA*turn/m)	Air flow (cm/s)	k (10 ³ cm/s)
1	0.00	0.00	1.81
2	0.00	0.27	2.69
3	0.00	0.68	3.19
4	4.28	0.00	2.85
5	4.28	0.27	3.46
6	4.28	0.68	3.92
7	7.71	0.00	2.99
8	7.71	0.68	4.77
9	7.71	0.97	5.60
10	11.2	0.00	3.50
11	11.2	0.27	4.78
12	11.2	0.68	4.50
13	11.2	1.17	4.93

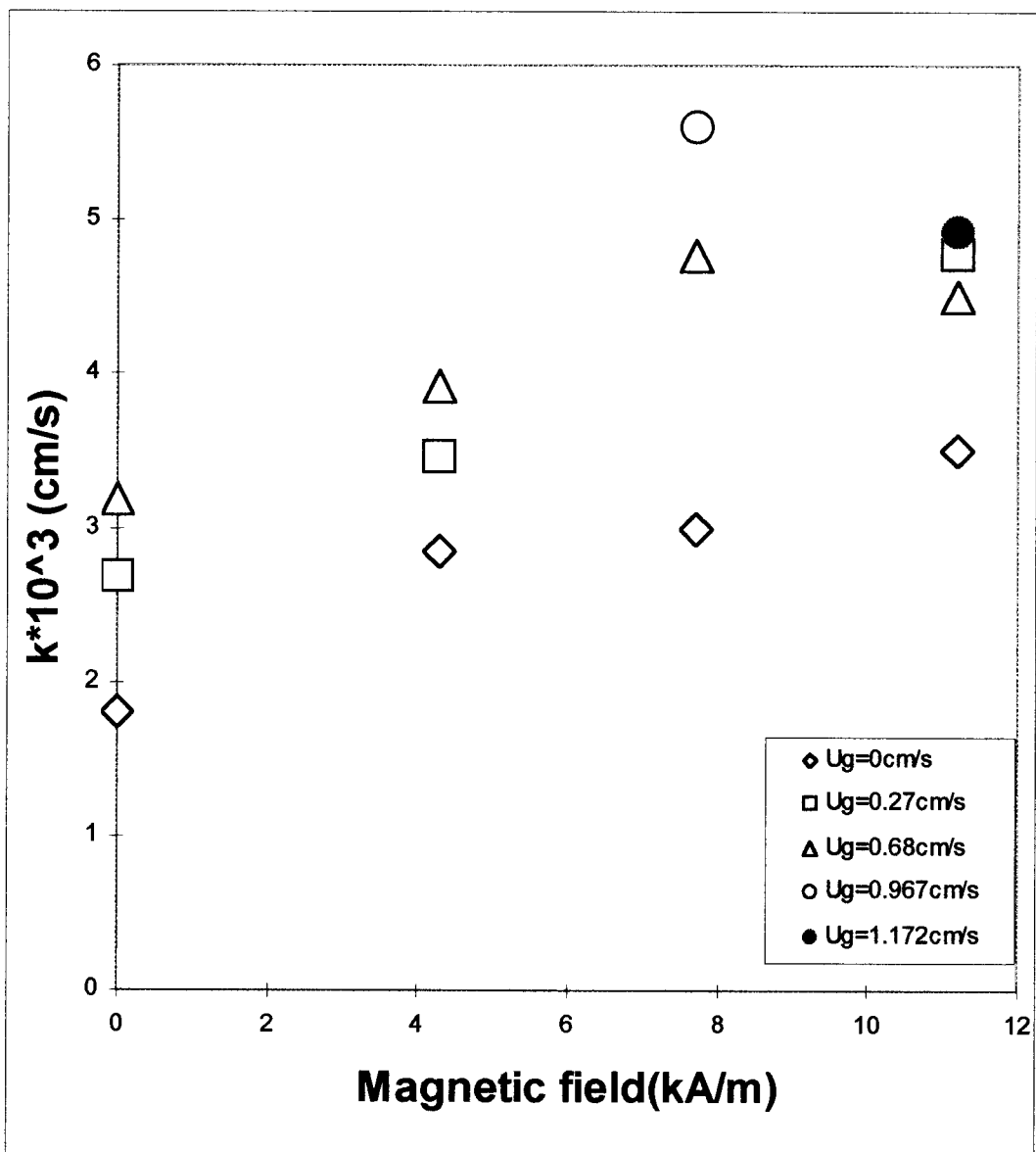


Figure 5-3 Mass Transfer Coefficient k as a Function of H for Different Gas Velocity

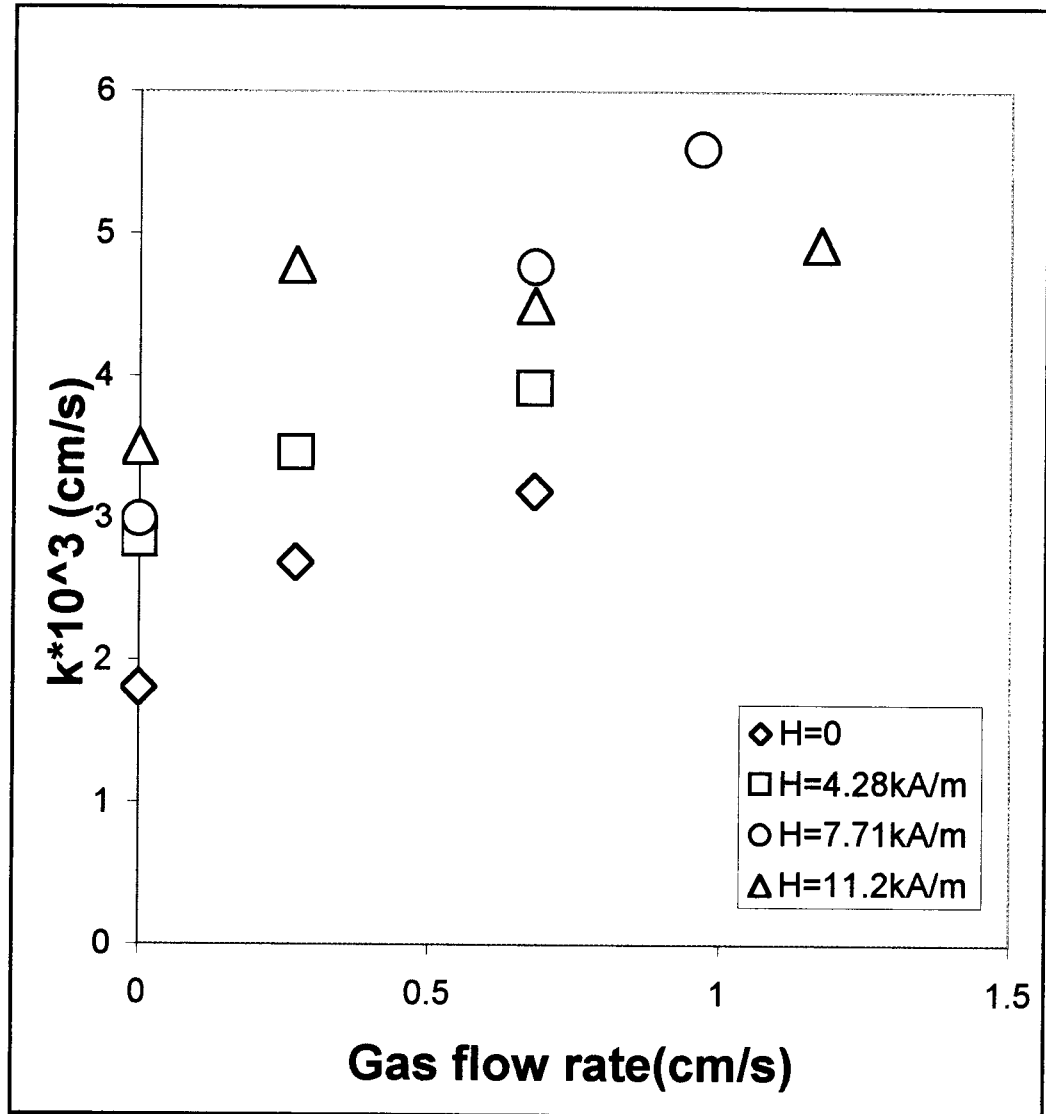


Figure 5-4 Mass Transfer Coefficient k as a Function of Gas Velocity for Different H

5.2.1 Discussion

From Figures 5-3 and 5-4, it can be concluded that

- For a given liquid and gas velocity in the experimental range (Figure 5-3), mass transfer coefficient k increases as magnetic field intensity increases. This is exactly what we expected and it is believed that this is caused by the decrease of the liquid porosity which leads to the increase in energy dissipation. As the liquid porosity decreases the liquid interstitial velocity must increase and higher liquid-particle relative velocity will result in a better mass transfer.
- For a given liquid velocity and magnetic field in the experimental range (Figure 5-4), the mass transfer coefficient k increases as the gas velocity increases. This result is the same as for the conventional three-phase fluidized bed operated with relatively high bed porosities. In conventional three-phase fluidized bed, the increase of the gas phase increases the energy dissipation, which results in the larger mass transfer coefficient k .

One thing we should pay attention to is the fact that, at a relatively higher gas velocity and magnetic field intensity, there is a possibility of reversing the rising trend of the mass transfer coefficient k . Fukuma (1988) claimed that in the packed bed regime of the three-phase fluidized bed at a small liquid flow rate and at high gas flow rate, the value of k decreased with increasing U_g . He also claimed, in this operational condition, large gas slugs ascend frequently and entirely cover the active particles, so that the effective liquid-solid contact area may decrease, thus decreasing the overall mass transfer rate. This regime may apply to two of the experimental points (run 12 and 13), but more experimental data are needed to confirm this, which will be a part of the

recommendation. However, this regime is not of our immediate interest since it is in contradiction to our major goal.

5.3 Mass Transfer Coefficient Correlation

The following describes the method of finding the correlation of mass transfer coefficient k with the magnetic field H . The parameters are assumed to be constants throughout the experiments:

Fluid kinematic viscosity, ν of the liquid (water)=0.01 [cm^2 / s]

Diffusion coefficient of MB into the water, $D=3.6 \times 10^{-6}$ [cm^2 / s]

(the calculation of D is shown in Appendix J)

First, it is confirmed, although three mass transfer coefficient k data obtained without a magnetic field appear a little higher than the k values from other researchers (Figure 5-5), these data are all in the same range as Arters and Fan's data (1986).

Therefore it is decided the modified Kawase equation, which fits best among the two correlations (3-1) and (3-2), can be used. From equation (3-1),

$$Sh = 0.01224(Ed_p^4 / \nu_l^3)^{0.45} Sc^{1/3} \quad \text{modified Kawase Equation} \quad (5-10)$$

The two modified constants in this modified equation are found by minimizing the sum of squared differences between the measured and calculated values. Runs 12 and 13, where the trend of increasing k with the increase of the magnetic field is reversed, are excluded.

Second, the plotting was extended to all the data with magnetic field applied. However, as shown on Figure 5-6, our experimental data appeared to exceed expected

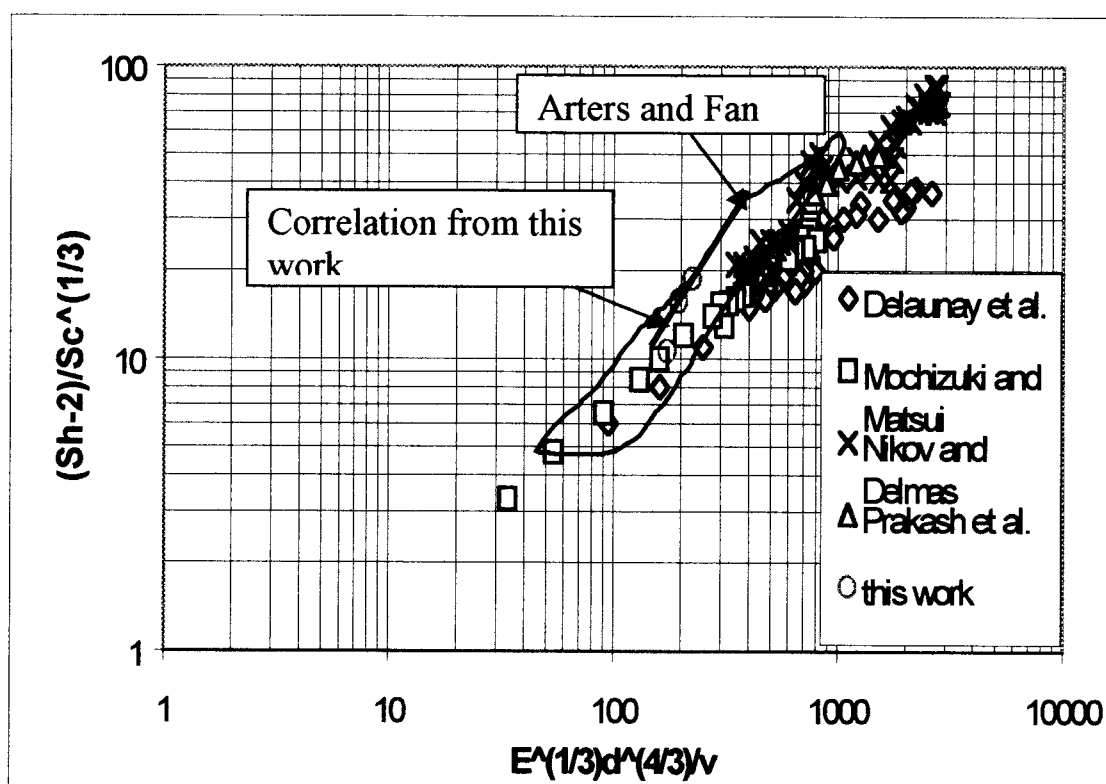


Figure 5-5 Comparison of This Work with Other Published Data on k in Three-phase Fluidized Beds and in Packed Beds with Gas-Liquid Upflow

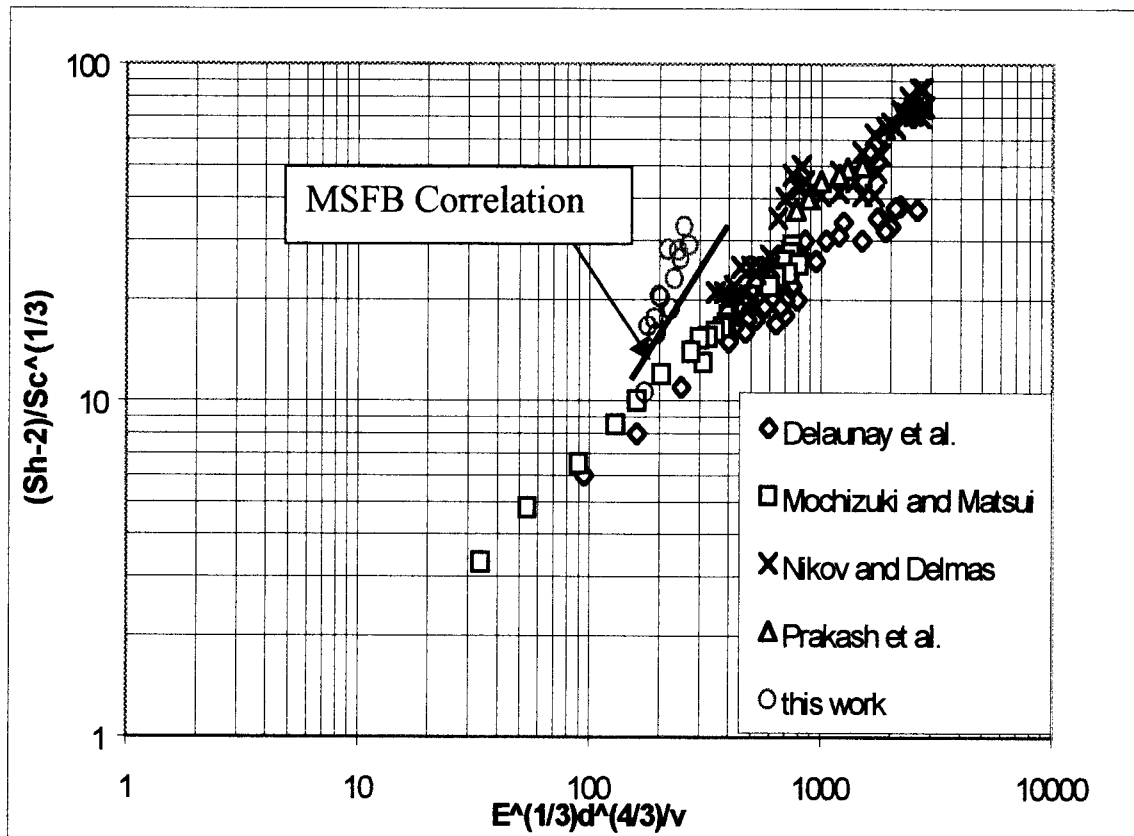


Figure 5-6 Possibility of Introducing the New Term in Energy Dissipation E

values that would be obtained from modified Kawase equation, as well as all the other contributions. This means there is a possibility of higher energy dissipation caused by the influence of the magnetic field. Increased energy dissipation is caused by a change in the bed structure, as well as by a decrease of the liquid porosity. These are the factors which affect the enhancement of the mass transfer coefficient k . Therefore, another term can be added to the energy dissipation term E in equation (3-3) to account for the influence of the magnetic field.

$$E = g\{(u_l + u_g)(\varepsilon_s \rho_p + \varepsilon_l \rho_l) - u_l \rho_l + \psi H\} / (\varepsilon_l \rho_l) \quad (5-11)$$

The coefficient ψ in the new term ψH is fitted to all available experimental data, with the same calculated procedure as is done in determining the coefficient in modified Kawase equation. The experimental value obtained for ψ is $0.12 \text{ [kg/kA} \cdot \text{m} \cdot \text{s}]$.

The graph using the modified energy dissipation term, E , is shown in Figure 5-7. The graph of the calculated k values versus the k values from the correlation prediction is also plotted in Figure 5-8.

5.3.1 Discussion

Although the experimental values for k seem to be a little higher than the k values from the correlation (especially when no magnetic field is applied), we were successful in finding a correlation that is close to the measured mass transfer coefficients. Both the measured and calculated k values have the same trend and most of all, the possibility of existence of a new term in energy dissipated E was confirmed. With a more resolute correlation between the liquid porosity and the magnetic field, for example, the one proposed by Honorez (1994), the mass transfer coefficient k can be predicted in three-phase MSFB.

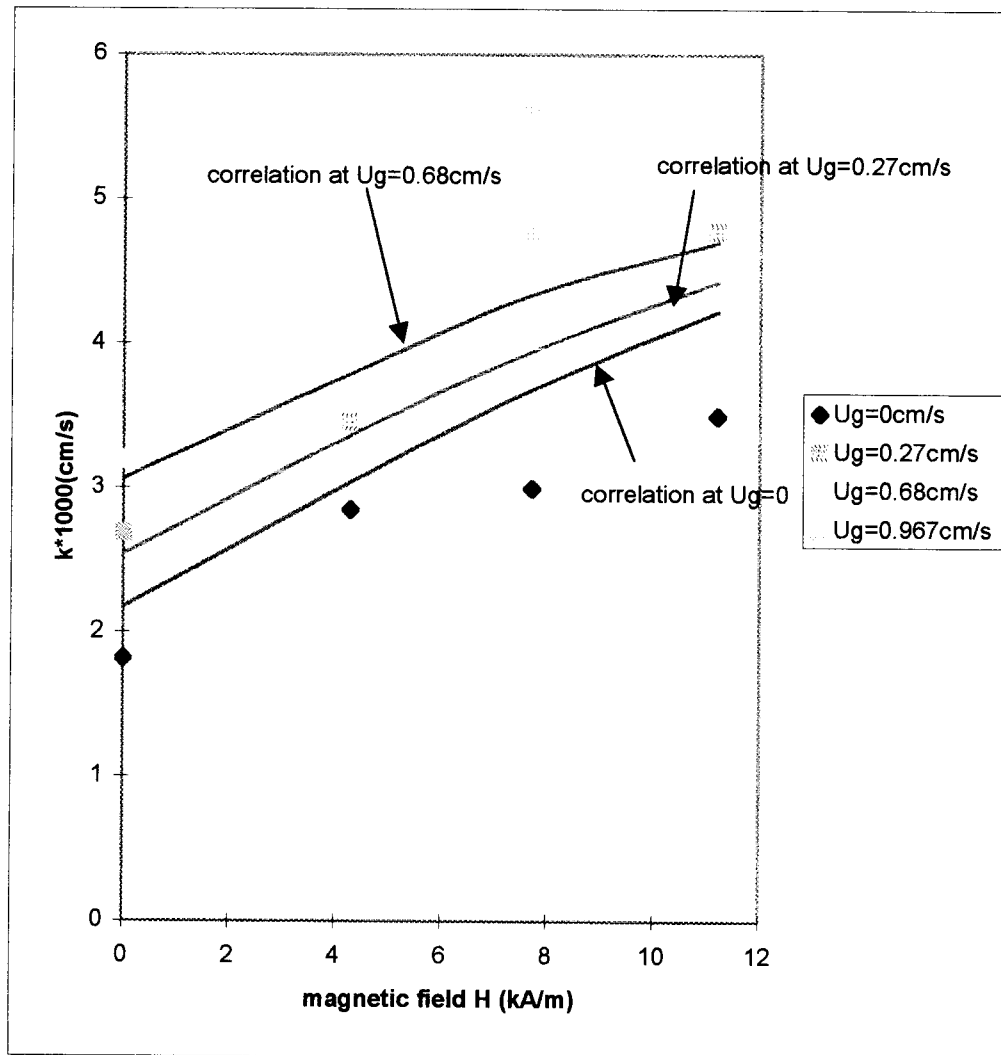


Figure 5-7 Correlations of the Mass Transfer Coefficient k with Magnetic Field H

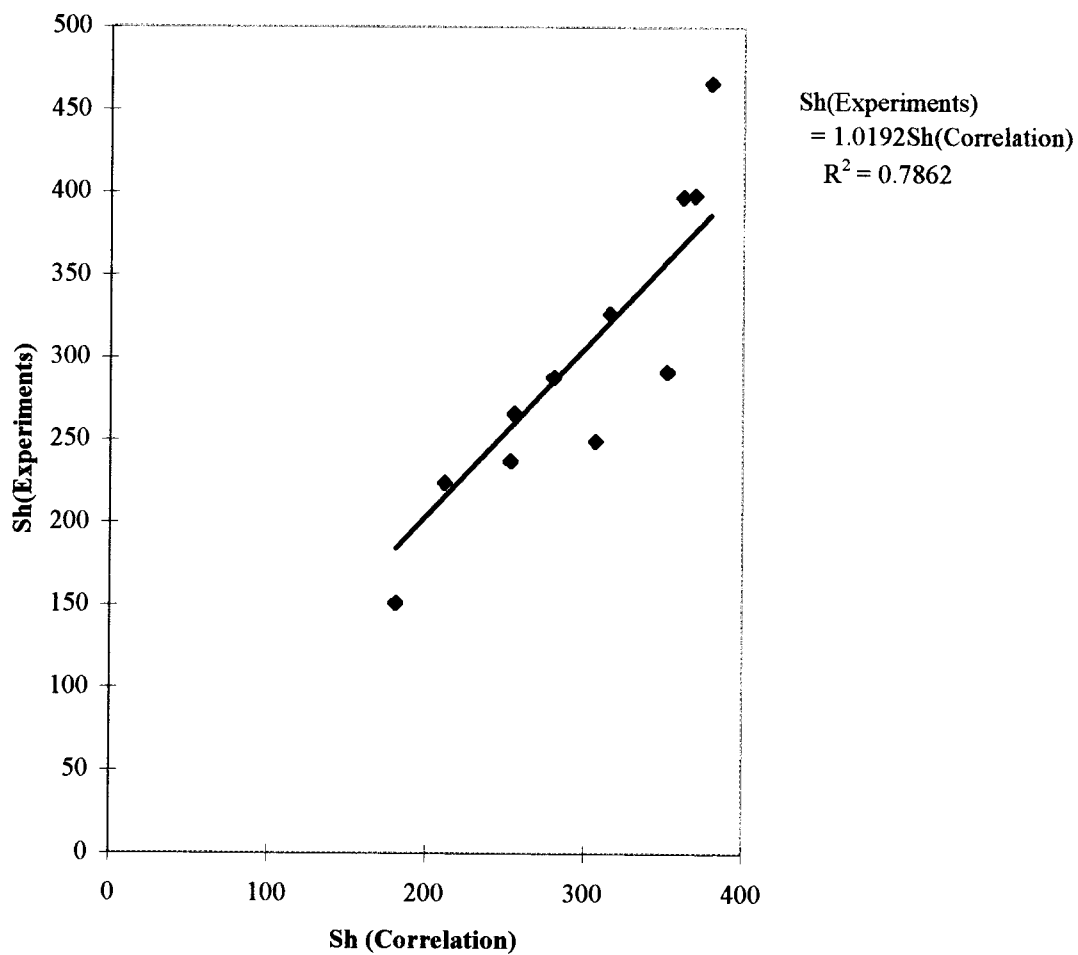


Figure 5-8 Sh from the Experiment versus Sh from Correlation Prediction

CHAPTER 6

CONCLUSION AND RECOMMENDATIONS

6.1. Conclusion

This study was conducted to produce original experimental concentration data using the adsorption of MB dye on ferromagnetic particles in three-phase MSFB. Experimental data that related the liquid porosity to the magnetic field intensity, liquid flow rate and gas flow rate in three-phase MSFB were also produced. The data were used to confirm the enhancement of liquid-solid mass transfer coefficient by the magnetic field in three-phase MSFB.

This study used the mathematical model proposed by Al-Mulhim (1995) and it was used to calculate the mass transfer coefficient for the adsorption for MB on the fluidizing particles. The model was solved analytically, and mass transfer coefficient was calculated using this form of the solution:

$$\ln\left\{\frac{C(1+mK_e)-C_0}{C_0(1+mK_e)-C_0}\right\} = \frac{1+mK_e}{mK_e} \frac{F}{V} (e^{-\alpha t} - 1)t \quad (3-10)$$

The mathematical model solution, and hence the calculation of mass transfer coefficient, was based on the initial adsorption data in which the diffusion resistance was neglected and the particle concentration was assumed to be constant.

The trend of liquid porosity-magnetic field intensity data was found to coincide with the previous studies conducted by Kwauk (1992), Jovanovic et al.(1993) and Honorez (1994) although they were conducted in two-phase MSFB.

$$\varepsilon_l = \varepsilon_{l,ms} + (\varepsilon_{l,ff} - \varepsilon_{l,ms}) \exp(-(1 - \varepsilon_l)(\alpha H + \beta) \frac{H}{H_{ms}}) \quad \text{Honorez (1994)} \quad (5-2)$$

However, the parameters used in the equations (for example, ε_{ff} , ε_{ms} and H_{ms} in Equation (5-2)) depend on the gas flow rate as well as on the liquid flow rate. Further investigation might be needed for these parameters.

The most important conclusion of this study was the enhancement of liquid-solid mass transfer coefficient by the magnetic field in three-phase MSFB. The combining effect of the gas agitation and the magnetic field enhanced the mass transfer coefficient even greater than when the gas agitation or the magnetic field are applied separately. It is believed that the enhancement with the application of the magnetic field is not only because of the increase of the interstitial liquid velocity but also because of some kind of structural change with the application of the magnetic field. Both effects result in the increase of the energy dissipated although not much is known about the structure.

A correlation that relates mass transfer coefficient to the magnetic field, liquid flow and the gas flow was proposed. The correlation is:

$$Sh = 0.01224(Ed_p^4 / \nu_l^3)^{0.45} Sc^{1/3} \quad (5-10)$$

where

$$E = g\{(u_l + u_g)(\varepsilon_s \rho_p + \varepsilon_l \rho_l) - u_l \rho_l + 0.12H\} / (\varepsilon_l \rho_l) \quad (5-11)$$

This correlation is analogous to the correlation proposed by Kawase et al. (1987). The fit of the experimental data into equation (5-10) is convincing.

6.2 Recommendations

For further studies, the following points are recommended.

1- Higher gas velocity can be attempted to see if mass transfer coefficient is will decrease in relatively high combination of gas velocity and magnetic field. If it proves to be true, regime map diagram can be attempted. To accomplish this, it would be much realistic to try the experiments at lower liquid velocities.

2- A field gradient with weaker magnetic field on the top of the bed, will make possible the infinitely increasing liquid superficial velocity. It's the same effect as using the infinitely heavy particles, which will increase the liquid-solid mass transfer coefficient significantly.

3- There should be much further investigation on the structure of three phase MSFB, for example, including, as suggested above, relationship of the liquid porosity and the magnetic field. It will pave the way to find what the extra term in the energy dissipated E really could be. One possibility is the consideration of tortuosity factor.

BIBLIOGRAPHY

Al-Mulhim and Jovanovic, G., Enhancement of Mass Transfer Coefficient in A Liquid-Solid Fluidized Bed, M.S. Thesis (1995)

Arnaldos, J., Casal, J., Lucas, A. and Puigjaner, L., Magnetically Stabilized Fluidization: Modelling and Application to Mixtures, Powder Technology, 44 (1985) 57-62

Arters, D. and Fan, L.S., Solid-Liquid Mass Transfer in A Gas-Liquid-Solid Fluidized Bed, Chem.Eng. Science, Vol. 41, No.1. pp. 107-115 (1986)

Arters, D. and Fan, L.S., Experimental Methods and Correlation of Solid-Liquid Mass Transfer in Fluidized Beds, Chem.Eng. Science, Vol. 45, No.4. pp. 965-975 (1990)

Briens, L.A., Briens, C.L., Margaritis, A. and Hay, J., Minimum Liquid Fluidization Velocity in Gas-Liquid-Solid Fluidized Beds, AIChE Journal, Vol. 43, No.5., 1180-1189 (1997)

Burns, M. A., Graves, D. J., Structural Studies of a Liquid-fluidized Magnetically Stabilized Bed, Chem. Eng. Comm. Vol. 67 (1988), pp 315-30

Casal, J., Arnaldos, J., The Structure of Magnetized-Fluidized Beds, Powder Technology, 64 (1991) 43-48

Edgar, T.F., Himmelblau, D.M., Optimization of Chemical Processes, McGraw-Hill (1988)

Fan, L.S., Gas-Liquid-Solid Fluidization Engineering, Butterworths (1989)

Fee, C., Stability of the Liquid-Fluidized Magnetically Stabilized Fluidized Bed, AIChE Journal, May 1996, Vol. 42, No. 5, 1213-1219

Filippov, M.V., The Effect of Magnetic Field on a Ferromagnetic Particle Suspension Bed, Pric. Magnet. lat.SSR, 12, 215 (1960)

Foscolo, P. U., Gibilaro, L.G., Felice, R.D., Waldram, S.P., The Effect of Interparticle Forces on the Stability of Fluidized Beds, Chemical Engineering Science, Vol. 40, No. 12, pp. 2379-2381 (1985)

Fukuma, M., Sato, M., Muroyama, K. and Yasunishi, A., Particle-to-Liquid Mass Transfer in Gas-Liquid-Solid Fluidization, J.Chem.Eng.Japan, Vol.21, No.3. (1988)

Furusawa, T. and Smith J.M., Fluid-Particle and Interparticle Mass Transport Rates in Slurries, Ind. Eng. Chem. Fundam., 12, No.2. 197 (1973)

Geuzens,P. and Thoenes,D., Magnetically Stabilized Fluidization; Part 1 Gas and Solids flow, Chem.Eng. Comm., Vol.67. pp217-228 (1988)

Goetz, V., and Graves, J., Axial Dispersion in a Magnetically Stabilized Fluidized Bed Liquid Chromatography Column, Powder Technology, 64 (1991) 81-92

Haas,P.A., Formation of Liquid Drops with Uniform and Controlled Diameters at Rates of 10^3 to 10^5 Drops Per Minute, AIChE Journal, Vol 21., No 2., 383-385 (1975)

Honorez, L. and Jovanovic, G., Fluid Dynamic Characteristics of a Magnetically Stabilized Fluidized Bed, M.S. Thesis (1994)

Hristov, J. Y., Fluidization of ferromagnetic particles in a magnetic field Part 1: The effect of field line orientation on bed stability, Powder Technology 87 (1996) 59-66

Jamialahmadi,M., Malayeri,M.R. and Muller-Steinhagen,H., Prediction of Optimum Operating Conditions of Liquid Fluidized Bed Systems, Canadian Journal of Chem.Eng., Vol 75, 327-332 (1997)

Kikuchi,K., T. Sugawara and H.Ohashi, Correlation of Mass Transfer Coefficient Between Particles and Liquid Fluidized Beds, J. Chem.Eng.Japan Vol.16. No.5., 426-428 (1983)

Kikuchi,K., Takahashi, H. and T. Sugawara, Liquid-Solid Mass Transfer in a Slurry Bubble Column and a Gas-Liquid-Solid Three-Phase Fluidized Bed, Canadian Journal of Chem.Eng., Vol.73.313-321 (1995)

Kundakovic, Lj. and Vunjak-Novakovic, G., Mechanics of Particle Motion in Three-phase Flow, Chem. Eng. Science, Vol.50, No. 20, pp. 3285-3295 (1995)

Kunii, D. and Levenspiel, O., Fluidization Engineering, Wiley, New York (1991)

Kwauk, M., Ma, X., Ouyang, F., Wu, Y., Weng, D. and Cheng, L., Magnetofluidized G/L/S Systems, Chemical Engineering Science, Vol. 47. No.13/14, pp.3467-3474 (1992)

Liu, Y. A., Hamby, R. K. and Colberg, D., Fundamental and practical Developments of magnetofluidized Beds: a Review, powder Technology, 64 (1991) 3-41

Muroyama,K. and Fan,L.S., Fundamentals of Gas-Liquid-Solid Fluidization, AIChE Journal, Vol.31. No.1., 1-34 (1985)

Penchev, I.P., and Hristov, J. Y., Behaviour of Fluidized Beds of Ferromagnetic Particles in an Axial Magnetic Field, Powder Technology, 61 (1990) 103-118

Rosensweig, R. E., Magnetic Stabilization of the State of Uniform Fluidization, Ind. Eng. Chem. Fundam., Vol. 18, No. 3 (1979)

Rosensweig, R. E., Fluidization: Hydrodynamic Stabilization with a Magnetic Field, Science, Vol. 204 (1979)

Sajc, L., Jovanovic, G., Jovanovic, Z. and Bugarski, B., Liquid Dispersion in a Magnetically Stabilized Fluidized Bed (MSFB), Mixed-Flow Hydrodynamics-Advances in Engineering Fluid Mechanics Series, Chapter 31, 713-740 (1996)

Sajc, L., Jovanovic, Z., Jovanovic, G., Bugarski, B. and Vunjak-Novakovic, G., The Interfacial Stability of Magnetically Stabilized Fluidized Beds, J. Serb. Chem. Soc. 61 (4-5) 319-329 (1996)

Saxena, S. C. and Shrivastava, S., Some Hydrodynamic Investigations of a Magnetically Stabilized Air-Fluidized Bed of Ferromagnetic Particles, Powder Technology 64 (1991), 57-67

Siegell, J. H., Liquid-Fluidized Magnetically Stabilized Beds, Powder Technology, 52 (1987) 139-148

Siegell, J. H., Magnetically Frozen Beds, Powder Technology, 55 (1988) 127-132

Siegell, J. H., Early Studies of Magnetized-Fluidized Beds, Powder Technology, 57 (1989) 213-220

Terranova, B. E., Burns, M. A., Continuous Cell Suspension Processing Using Magnetically Stabilized Fluidized Beds, Biotechnology and Bioengineering, Vol. 37, pp. 110-120 (1991)

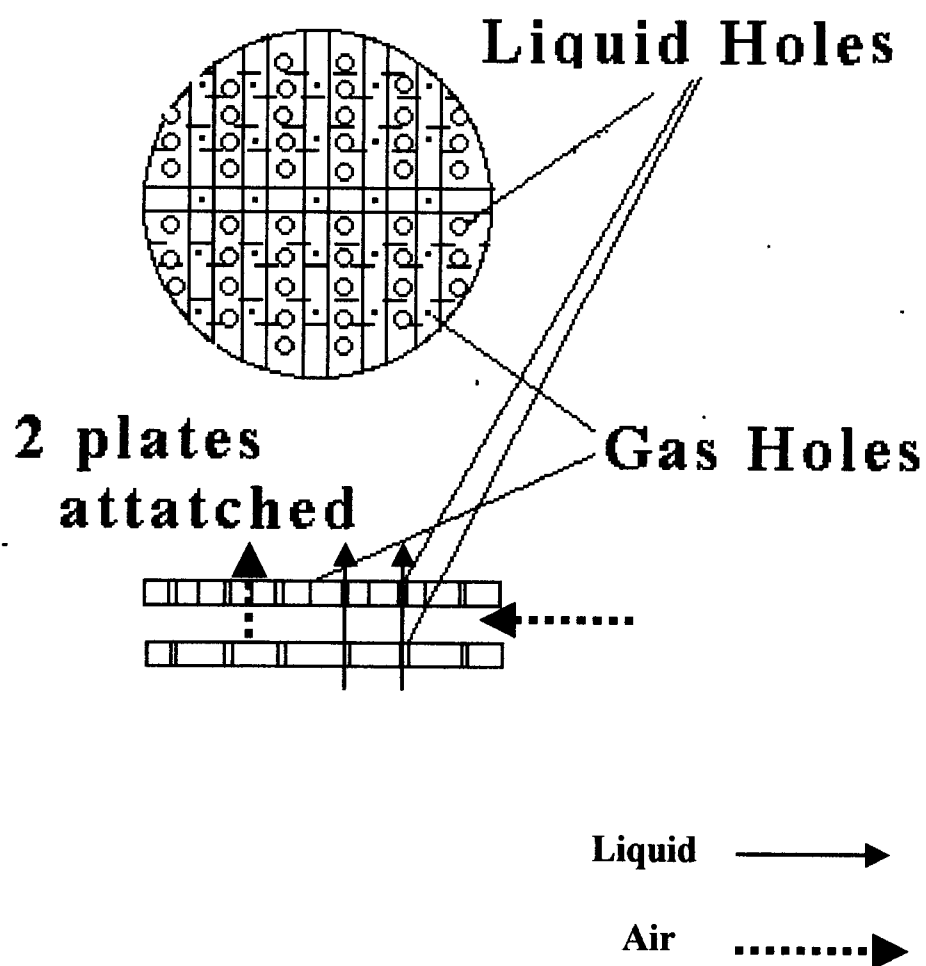
Tournie, P., Laguerie, C. and Couderc, J. P., Correlations for Mass Transfer Between Fluidized Spheres and a Liquid, Chemical Engineering Science Vol. 34, pp. 1247-1255

Villers, F., Bed Porosity of the Magnetically Stabilized Two-phase Fluidized Bed, M.S. Thesis (1998)

Wheeler, J. M., Middleman, S., Machine Computation of Transients in Fixed Beds with Intraparticle Diffusion and Nonlinear Kinetics, Ind. Eng. Chem. Fundam., Vol. 9, No. 4 (1970) 624-627

APPENDICES

APPENDIX A
DESIGN OF THE DISTRIBUTOR PLATE



APPENDIX B

PARTICLES PRODUCTION

The particles used in this study are composite ferromagnetic particles, which are made of mixture of alginate, activated carbon and ferrite powder. The particles production schematic diagram is shown in Figure B-1.

Preparation of the ferromagnetic sodium alginate suspension:

The preparation of the ferromagnetic sodium alginate is given by the following instructions:

- 1- Weigh a 393 [g] amount of distilled water and place the beaker under the mixer,
- 2- Weigh a 7 [g] amount of sodium alginate powder that will constitute 1.75% of the total weight of water + alginate,
- 3- Start mixing the water and add the alginate powder to the water in a small increments away from the mixer until all alginate powder is added to the water,
- 4- Mix the solution for about 20 minutes.
- 5- Weigh the amount of ferrite powder and activated carbon that will constitute 20%, 10%, respectively, of the total weight of alginate solution
- 6- Add the ferrite powder and activated carbon to the alginate suspension in a small increments while stirring the mixture,
- 7- Repeat step 6 until all ferrite powder and activated carbon are added and a uniform suspension is obtained.

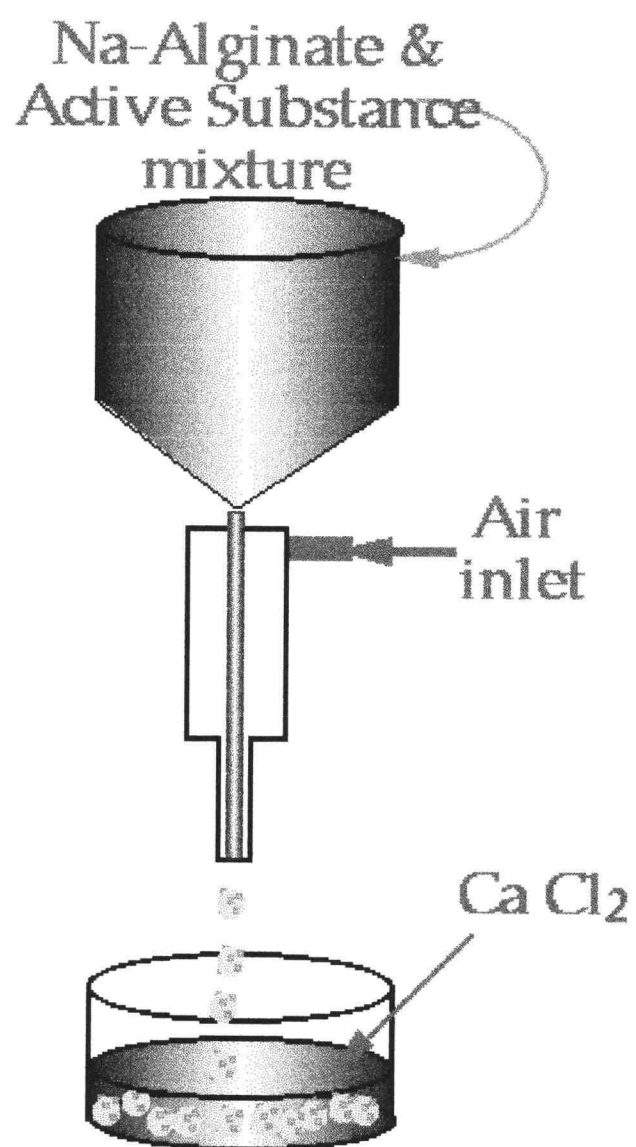


Figure B-1 Extrusion of the Particles

Mechanism of alginate droplet formation :

The mechanism of alginate droplet formation and experimental parameters for their production depend on incoming air flux rate in the particle generator, the pressure in the vessel, alginate solution viscosity and surface tension.

The particle size is adjusted by regulating the pressure drop and the air flow, which is used to shear the particles off the needle. Increasing the incoming flux rate of air inlet in the particle generator, we can produce smaller particles. Decreasing the pressure in the vessel, we can generate smaller particles. After the vessel is pressurized, the liquid meniscus at the tip needle is distorted from a spherical shape into an inverted cone-like shape. Hence, alginate solution flows into this cone at an increasing rate causing formation of a neck-like filament. Filament breaks away, producing droplets, the meniscus relaxed back to a spherical shape until flow of the alginate caused the process to start again. The particles obtained in the particle generator are roughly of the same size if parameters (pressure, viscosity and air flow) are kept constant.

The average particles size is determined by weight method. Once we know the density, the number and the mass of a given number of particles and assuming perfect spherical shape we can calculate the average diameter of particles.

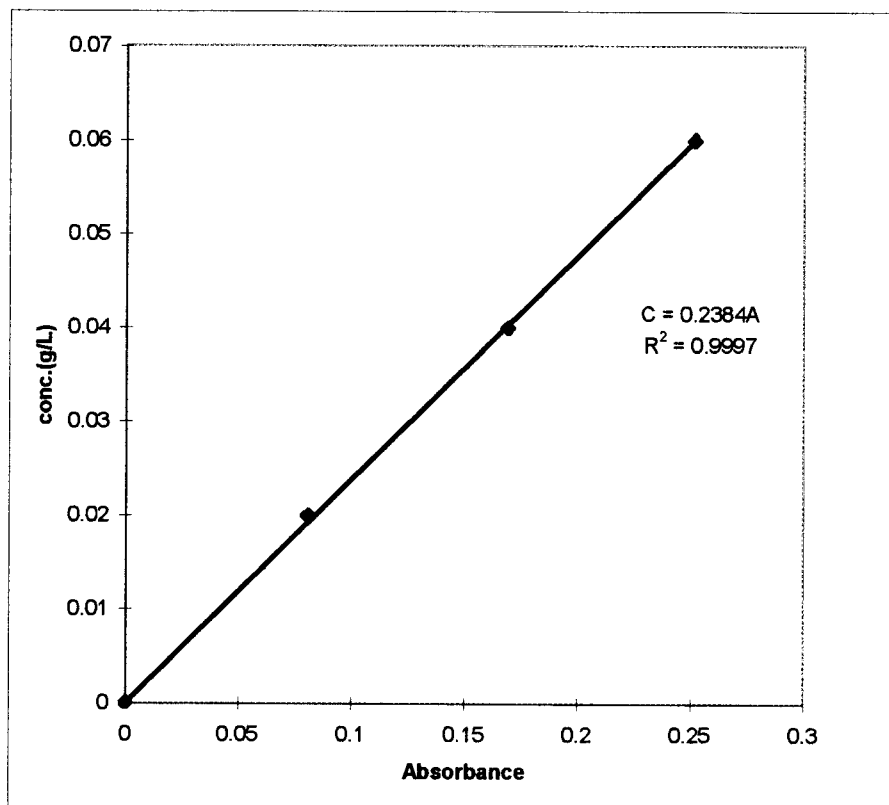
The properties of the alginate sodium and ferromagnetic powder are given in Table B-1.

Table B-1 Ferrite and Alginate Properties

Material	Powder Size (mm)	True density [kg/m ³]
Ferrite	6	4
Keltone HV (sodium alginate)	180	1.59

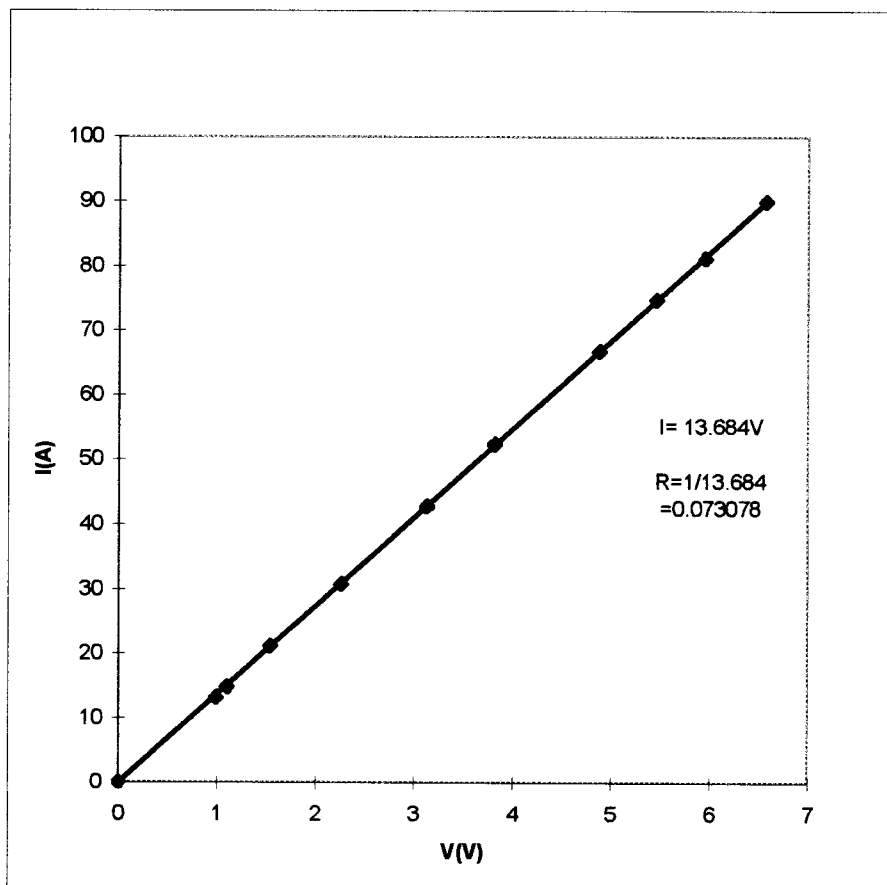
APPENDIX C

COLORIMETER CALIBRATION CURVE



APPENDIX D

VOLTAGE VS. CURRENT CALIBRATION CURVE



APPENDIX E

NUMERICAL METHOD

FOR SOLVING MATHEMATICAL MODEL

```

PROGRAM thesis optimization
INTEGER NDIM
C REAL FTOL
DOUBLE PRECISION FTOL, cexp, func
PARAMETER (NDIM=2, FTOL=1.0E-6)
INTEGER i, iter, np, kt2, nt, mt
C REAL fret, p(NDIM), xi(NDIM, NDIM)
DOUBLE PRECISION p(NDIM), xi(NDIM, NDIM), fret
common cexp(20), kt2(20), mt
nt=1
open(unit=1, file='rrun1.txt', status='old')
13 read(1, *, end=25) kt2(nt), cexp(nt)
c print *, kt2(nt), nt
nt=nt+1
goto 13
25 mt=nt-1
np=NDIM
c print *, cexp(2), kt2(2), mt
c print *, mt
c DATA xi/1.0, 0.0, 0.0, 0.0, 1.0, 0.0, 0.0, 0.0, 1.0/
c DATA p/1E-9, 5.35E-5, 1.0/
DATA xi/1.0, 0.0, 0.0, 1.0/
DATA p/1.83E-9, 5.45E-5/
call powell(p, xi, NDIM, np, FTOL, iter, fret)
write(*, '(1x, a, i3)') 'Iterations:', iter
write(*, '(1x, a/1x, 2f12.6)') 'Minimum found at: ', (p(i), i=1, NDIM)
write(*, '(1x, a, f12.6)') 'Minimum function value =', fret
c write(*, '(1x, a)') 'True minimum of function is at:'
c write(*, '(1x, 3f12.6/)') 1.0, 2.0, 3.0
END
C*****
SUBROUTINE powell(p, xi, n, np, ftol, iter, fret)
DOUBLE PRECISION p(np), xi(np, np), ftol, fret, pt(20), del, xit(20)
+, fp, t, func

INTEGER iter, n, np, NMAX, ITMAX
C REAL fret, ftol, p(np), xi(np, np), func
c EXTERNAL func
PARAMETER (NMAX=20, ITMAX=200)
CU USES func, linmin
INTEGER i, ibig, j
C REAL del, fp, fptt, t, pt(NMAX), ptt(NMAX), xit(NMAX)
fret=func(p)
do 11 j=1, n
pt(j)=p(j)
11 continue
iter=0
1 iter=iter+1

c WRITE(*, 114) FRET, (p(I), I=1, 3)
c 114 FORMAT(1X, 'FUNC=', E10.3, ' del1=', f6.3,

```

```

c      + ' del2=',f6.3,' del3=',f6.3)

      fp=fret
      ibig=0
      del=0.
      do 13 i=1,n
        do 12 j=1,n
          xit(j)=xi(j,i)
12      continue
          fptt=fret
          call linmin(p,xit,n,fret)
          if(abs(fptt-fret).gt.del) then
            del=abs(fptt-fret)
            ibig=i
          endif
13      continue
          if(2.*abs(fp-fret).le.ftol*(abs(fp)+abs(fret))) return
c      IF(fret.LE.0.1) RETURN
          if(iter.eq.ITMAX) then
            pause 'powell exceeding maximum iterations'
            print 16,fret
16      format(1x,'fret=func=',e10.3)
          end if
          do 14 j=1,n
            ptt(j)=2.*p(j)-pt(j)
            xit(j)=p(j)-pt(j)
            pt(j)=p(j)
14      continue
            fptt=func(ptt)
            if(fptt.ge.fp) goto 1
            t=2.*(fp-2.*fret+fptt)*(fp-fret-del)**2-del*(fp-fptt)**2
            if(t.ge.0.) goto 1
            call linmin(p,xit,n,fret)
            do 15 j=1,n
              xi(j,ibig)=xi(j,n)
              xi(j,n)=xit(j)
15      continue
              goto 1
            return
          END
C*****
      SUBROUTINE linmin(p,xi,n,fret)
      DOUBLE PRECISION p(n),xi(n),TOL,fldim,fret,ax,bx,fa,fb,fx,xmin,
      +pcom(50),xicom(50),brent,xx

      INTEGER n,NMAX
C      REAL fret,p(n),xi(n),TOL
      PARAMETER (NMAX=50,TOL=1.e-4)
CU      USES brent,fldim,mnbrak
      INTEGER j,ncom
C      REAL ax,bx,fa,fb,fx,xmin,xx,pcom(NMAX),xicom(NMAX),brent
      COMMON /flcom/ pcom,xicom,ncom
      EXTERNAL fldim
      ncom=n
      do 11 j=1,n
        pcom(j)=p(j)
        xicom(j)=xi(j)
11      continue
      ax=0.
      xx=1E-8

```

```

c      xx=5
c      print 16,fret,(pcom(i),i=1,n)
c16      format(1x,'FUNC=',f7.3,' DELTA1:',3(3x,f10.4))

      call mnbrak(ax,xx,bx,fa,fx,fb,fldim)
c      print 17,(pcom(i),i=1,n)
c17      format(1x,'DELTA2:',3(3x,e10.3))

      fret=brent(ax,xx,bx,fldim,TOL,xmin)
      do 12 j=1,n
          xi(j)=xmin*xi(j)
          p(j)=p(j)+xi(j)
12      continue
c      print 15,(p(i),i=1,n)
c15      format(1x,'DELTA:',3(3x,f10.4))
      return
      END
C*****
      SUBROUTINE mnbrak(ax,bx,cx,fa,fb,fc,func)
      DOUBLE PRECISION ax,bx,cx,fa,fb,fc,func,GOLD,GLIMIT,TINY,dum,fu,
+ q,r,u,ulim

C      REAL ax,bx,cx,fa,fb,fc,func,GOLD,GLIMIT,TINY
      EXTERNAL func
      PARAMETER (GOLD=1.618034, GLIMIT=100., TINY=1.e-20)
C      REAL dum,fu,q,r,u,ulim
      fa=func(ax)
      fb=func(bx)
      if(fb.gt.fa)then
          dum=ax
          ax=bx
          bx=dum
          dum=fb
          fb=fa
          fa=dum
      endif
      cx=bx+GOLD*(bx-ax)
      fc=func(cx)
1      if(fb.ge.fc)then
          r=(bx-ax)*(fb-fc)
          q=(bx-cx)*(fb-fa)
          u=bx-((bx-cx)*q-(bx-ax)*r)/(2.*sign(max(abs(q-r),TINY),q-r))
          ulim=bx+GLIMIT*(cx-bx)
          if((bx-u)*(u-cx).gt.0.)then
              fu=func(u)
              if(fu.lt.fc)then
                  ax=bx
                  fa=fb
                  bx=u
                  fb=fu
                  return
              else if(fu.gt.fb)then
                  cx=u
                  fc=fu
                  return
              endif
              u=cx+GOLD*(cx-bx)
              fu=func(u)
          else if((cx-u)*(u-ulim).gt.0.)then
              fu=func(u)

```

```

        if(fu.lt.fc)then
            bx=cx
            cx=u
            u=cx+GOLD*(cx-bx)
            fb=fc
            fc=fu
            fu=func(u)
        endif
        else if((u-ulim)*(ulim-cx).ge.0.)then
            u=ulim
            fu=func(u)
        else
            u=cx+GOLD*(cx-bx)
            fu=func(u)
        endif
        ax=bx
        bx=cx
        cx=u
        fa=fb
        fb=fc
        fc=fu
        goto 1
    endif
    return
END
C*****
      FUNCTION brent(ax,bx,cx,f,tol,xmin)
      DOUBLE PRECISION tol,f,ax,bx,xmin,cx,a,b,d,e,etemp,fu,fv,fw,fx,p
      +,q,r,toll,tol2,u,v,w,x,xm,brent,CGOLD,ZEPS

      INTEGER ITMAX
C      REAL brent,ax,bx,cx,tol,xmin,f,CGOLD,ZEPS
      EXTERNAL f
      PARAMETER (ITMAX=100,CGOLD=.3819660,ZEPS=1.0e-10)
      INTEGER iter
C      REAL a,b,d,e,etemp,fu,fv,fw,fx,p,q,r,toll,tol2,u,v,w,x,xm
      a=min(ax,cx)
      b=max(ax,cx)
      v=bx
      w=v
      x=v
      e=0.
      fx=f(x)
      fv=fx
      fw=fx
      do 11 iter=1,ITMAX
          xm=0.5*(a+b)
          toll=tol*abs(x)+ZEPS
          tol2=2.*toll
          if(abs(x-xm).le.(tol2-.5*(b-a))) goto 3
          if(abs(e).gt.toll) then
              r=(x-w)*(fx-fv)
              q=(x-v)*(fx-fw)
              p=(x-v)*q-(x-w)*r
              q=2.*(q-r)
              if(q.gt.0.) p=-p
              q=abs(q)
              etemp=e
              e=d
              if(abs(p).ge.abs(.5*q*etemp).or.p.le.q*(a-x).or.p.ge.q*(b-x))

```

```

*goto 1
    d=p/q
    u=x+d
    if(u-a.lt.tol2 .or. b-u.lt.tol2) d=sign(tol1,xm-x)
    goto 2
endif
1    if(x.ge.xm) then
        e=a-x
    else
        e=b-x
    endif
    d=CGOLD*e
2    if(abs(d).ge.tol1) then
        u=x+d
    else
        u=x+sign(tol1,d)
    endif
    fu=f(u)
    if(fu.le.fx) then
        if(u.ge.x) then
            a=x
        else
            b=x
        endif
        v=w
        fv=fw
        w=x
        fw=fx
        x=u
        fx=fu
    else
        if(u.lt.x) then
            a=u
        else
            b=u
        endif
        if(fu.le.fw .or. w.eq.x) then
            v=w
            fv=fw
            w=u
            fw=fu
        else if(fu.le.fv .or. v.eq.x .or. v.eq.w) then
            v=u
            fv=fu
        endif
    endif
11   continue
    pause 'brent exceed maximum iterations'
3    xmin=x
    brent=fx
    return
END
C*****
    FUNCTION fldim(x)
    DOUBLE PRECISION x,fldim,xt(50),pcom(50),xicom(50),func

    INTEGER NMAX
C    REAL fldim,func,x
    PARAMETER (NMAX=50)
CU   USES func

```

```

      INTEGER j,ncom
C      REAL pcom(NMAX),xicom(NMAX),xt(NMAX)
      COMMON /flcom/ pcom,xicom,ncom
      do 11 j=1,ncom
         xt(j)=pcom(j)+x*xicom(j)
11      continue
      fldim=func(xt)

      write(*,17) fldim,(xt(i),i=1,ncom)
17      format(1x,'func=',f7.3,'DELTAtry=',2(3x,e10.3))

      return
      END
C*****
      FUNCTION func(x)
      DOUBLE PRECISION x(2)
      real q(0:100,0:100,0:1900)
      double precision c(0:100,0:1900),cexp,func
      double precision a,e,b,v,vv,f,t0,dx,dr,dt,ap,L,R,U,D,h
      integer mm,jj,kk,kt2,mt
      integer ml,jl,kl,m,j,k,kt
      common cexp(20),kt2(20),mt
C      print *,cexp(2),kt2(2),mt
C      open(unit=8,file='thesis.out',status='unknown')
      e=0.731745
      L=0.213
      R=0.0015
      U=0.05
      D=x(1)
      h=x(2)
      v=h*R/D
      a=3*D*(1-e)*L/(R**2)/U
      b=1.0
      dx=0.1
      dr=0.1
      ap=e/3.0/(1.0-e)*a/990.1917
      f=0.00010415
      vv=0.014674
      t0=3.13
      dt=3.0/t0
      mm=10
      jj=10
      kk=1900

      do 1 ml=1,mm
         c(ml,0)=0.0
         do 10 jl=1,jj
            q(ml,jl,0)=0.0/b
10         continue
1      continue

         c(0,0)=0.06
C      print *,'results1 is',c(10,0),q(10,1,0),c(0,200)

C#####
      do 20 k=0,kk-1
         do 30 m=1,mm
            q(m,0,k)=q(m,1,k)
            if (k.eq.0) goto 31
            c(m,k)=(1.0/((v*dr*b+2.0)/

```

```

+          (2.0*v*b*a*dx)+1.0/b))
+          * ((v*dr*b+2.0)/(2.0*v*b*a*dx)
+          *c(m-1,k)
+          +q(m,jj,k))
c          print *, 'result 2 is', c(10,0)
31      q(m,jj+1,k)
+          =(2.0-v*dr*b)/(2.0+v*dr*b)
+          *q(m,jj,k)
+          +(2.0*v*dr)/(2.0+v*dr*b)
+          *c(m,k)
+      do 40 j=1,jj
+          q(m,j,k+1)
+          =q(m,j,k)
+          +dt*ap/(dr**2)
+          *(q(m,j+1,k)
+          -2.0*q(m,j,k)
+          +q(m,j-1,k)+2.0/(j-0.5)
+          *(q(m,j+1,k)
+          -q(m,j,k)))
40      continue

30      continue
+      c(0,k+1)=c(0,k)+(dt+dx)*t0*f/vv*(c(mm,k)-c(0,k))
c      print *,k*dt,c(0,k),c(10,k)
c      print *,k*dt,c(10,k)
c      write(8,*) k*dt*t0,c(0,k),c(10,k)
20      continue
c      print *,c(0,0),c(1,0),c(5,0),c(10,0)
c      + ,c(10,1)
+      func=0.0
c      print *,cexp(2),kt2(2),mt
+      do 21 kt=1,mt
c      print *,cexp(kt),kt2(kt),mt,func,c(0,kt2(kt)/3)
+      func=func+((cexp(kt)-c(0,kt2(kt)/3))/(cexp(kt)
+      +c(0,kt2(kt)/3)))**2
21      continue
c      print *,func
+      RETURN
+      END
C*****

```


APPENDIX F

DIFFUSION COEFFICIENT CALCULATION FROM NUMERICAL METHOD

As noted in section 3.2.3, numerical method was tried first to obtain simultaneously mass transfer and diffusion coefficients from the experimental data. However, diffusion coefficients calculated using this approach (Table F-1) are not only different from each other but also approximately an order of magnitude larger than the theoretical diffusion coefficient (see APPENDIX J).

run #	magn. Field (kA*turn/m)	air flow (cm/s)	k (10 ³ cm/s)	D (10 ⁵ cm ² /s)	obj.func*10 ³
1	0.00	0.00	1.81	6.16	1.281
2	0.00	0.27	2.69	6.28	0.007
3	0.00	0.68	3.19	3.71	5.302
4	4.28	0.00	2.85	8.04	7.444
5	4.28	0.27	3.46	3.88	4.229
6	4.28	0.68	3.92	3.17	6.831
7	7.71	0.00	2.99	4.73	1.307
8	7.71	0.68	4.77	3.19	7.830
9	7.71	0.97	5.60	3.23	8.522
10	11.2	0	3.50	4.31	5.311
11	11.2	0.27	4.78	2.43	8.869
12	11.2	0.68	4.50	2.61	5.383
13	11.2	1.17	4.93	2.3	6.390

It is believed that this error was caused by the lack of the resolution in the experimental measurement.

The purity of water used for liquid phase is also suspected to be one of the reason why we failed to obtain good diffusion coefficients. There could have been some impurities in water and multicomponent diffusion coefficient can be much different from the diffusion coefficient we intended to obtain.

APPENDIX G

ANALYTICAL SOLUTION FOR THE MODEL

From Chapter 4, combining equation (4-1) and (4-2) will lead to

$$C_{ss} = C_s = \frac{C_0 - C}{mK_e} \quad (G-1)$$

Taking into consideration the assumption that C_s is constant during one pass of the fluid through the fluidized bed, equation (3-8) can be integrated throughout the bed height L as:

$$\int_C^{C'} F \frac{dC^*}{C^* - C_s} = -ka' A \int_0^L dx$$

and it becomes

$$\text{Ln}\left\{\frac{C' - C_s}{C - C_s}\right\} = -\frac{ka' A}{F} L \quad (G-2)$$

Combining equations (G-1) and (G-2), we get

$$\text{Ln}\left\{\frac{C' - \frac{C_0 - C}{mK_e}}{C - \frac{C_0 - C}{mK_e}}\right\} = -\frac{ka' A}{F} L \quad (G-3)$$

Let $\alpha = \frac{a' AL}{F}$, then (G-3) can be rewritten as:

$$C' = \frac{C_0 - C}{mK_e} + \left\{C - \frac{C_0 - C}{mK_e}\right\} \exp(-\alpha k) \quad (G-4)$$

By combining (G-4) with equation (3-6), we obtain

$$F\left\{C - \frac{C_0 - C}{mK_e}\right\}\{e^{-\alpha k} - 1\} = V \frac{dC}{dt} \quad (G-5)$$

Equation (G-5) can be rearranged as

$$C(1 + mK_e) - C_0 = \left(\frac{V}{F}\right) \left\{ \frac{mK_e}{e^{-\alpha k} - 1} \right\} \frac{dC}{dt} \quad (G-6)$$

Equation (G-6) can be integrated to account for the total adsorbate concentration change throughout the system as

$$\int_{C_0}^C \frac{dC}{C(1 + mK_e) - C_0} = \frac{F}{V} \left\{ \frac{(e^{-\alpha k} - 1)}{mK_e} \right\} \int_0^t dt \quad (G-7)$$

Equation (G-7) can be integrated easily to obtain the final form as equation (3-10).

$$\text{Ln} \left\{ \frac{C(1 + mK_e) - C_0}{C_0(1 + mK_e) - C_0} \right\} = \frac{1 + mK_e}{mK_e} \frac{F}{V} (e^{-\alpha k} - 1)t \quad (3-10)$$

APPENDIX H

DYNAMIC PRESSURE P_d (in Pa) AT EACH PORT

(1Pa= 0.01 cmH₂O) at liquid flow rate=5cm/s

mag. field (kA/m)	air flow rate (cm/s)	Port1 (z=3.2 cm)	Port2 (z=8.4 cm)	Port3 (z=13.4 cm)	Port4 (z=18.5 cm)	Port5 (z=23.5 cm)	Port6 (z=28.6 cm)	port7 (z=33.7 cm)
0	0	101535	101485	101430	101385	101340	101300	101300
	0.27	101460	101420	101380	101340	101300	101270	101280
	0.68	101420	101385	101345	101315	101285	101255	101257
4.28	0	101520	101465	101410	101365	101315	101300	101300
	0.27	101458	101410	101360	101315	101270	101264	101276
	0.68	101425	101385	101345	101303	101260	101253	101262
7.71	0	101520	101460	101400	101340	101300	101300	101300
	0.68	101415	101365	101320	101272	101240		101246
	0.967	101410	101363	101321	101280	101243		101252
11.2	0	101515	101450	101380	101320	101300	101300	101300
	0.27	101470	101415	101355	101300	101280		101285
	0.68	101440	101385	101335	101285	101265		101270
	1.172	101380	101340	101300	101260	101235	101240	101245

APPENDIX I

CONCENTRATION MEASUREMENTS

I-1 : MB concentration measurement at $u_l = 5\text{cm/s}$ and $H = 0\text{kA/m}$

Time (min)	Air flow Velocity 0cm/s	Air flow velocity 0.27cm/s	Air flow velocity 0.68cm/s
0			
0.5			0.060032
1	0.056399	0.056399	0.059112
1.5		0.05551	0.058018
2	0.055333	0.055069	0.057295
2.5		0.053755	
3	0.054279	0.052889	0.055687
4	0.053408	0.052372	0.054279
5	0.052716		0.052458
6			
7	0.051177	0.049912	0.050754
8			
10	0.048249	0.045723	0.047837
15		0.043414	0.043492
15.5			
16			
18.5	0.042239		
25	0.039171	0.034372	0.035825
25.5			
40	0.032939	0.029785	0.031175
40.5			
41			
42.5			
59	0.028414		
60			
61		0.023103	0.026057
61.5			
62			
78.5	0.021817		
90	0.020547	0.01867	0.022137

I-2 : MB concentration measurements at $u_f = 5\text{cm/s}$ and $H = 4.28\text{kA/m}$

time (min)	Air flow velcoty 0cm/s	Air flow velcoty 0.27cm/s	Air flow velcoty 0.68cm/s
0			
0.5			0.059571
1	0.055953	0.058381	0.057295
1.5	0.055157		0.056042
2	0.054454	0.056399	0.055687
2.5		0.05498	0.05498
3	0.052889	0.054104	0.053929
4		0.053234	0.052889
5	0.049494	0.052372	
6	0.049077		
7		0.049494	0.048249
8	0.046207		
10	0.044283	0.047427	0.046856
15	0.041309	0.043021	
15.5			
16			0.041464
18.5			
25		0.037299	0.036486
25.5	0.034012		
40		0.033295	
40.5	0.025063		
41			0.029785
42.5			
59			
60	0.022073	0.024406	0.024406
61			
61.5			
62			
63.5			
78.5			
90		0.020547	0.021817
91	0.01836		

I-3 : MB concentration measurements at $u_f = 5\text{cm/s}$ and $H = 7.71\text{kA/m}$

time (min)	Air flow velocity 0cm/s	Air flow velocity 0.68cm/s	Air flow velocity 0.967cm/s
0			
0.5	0.057837	0.058746	0.057295
1	0.056399	0.056936	0.055069
1.5	0.05551	0.055865	0.054279
2	0.055157	0.055157	0.052889
2.5			
3	0.053755	0.052458	
4	0.05203	0.051177	
5	0.050838		0.049494
6			
7	0.048994	0.047019	0.046207
8			
10	0.046612	0.045	0.043178
15	0.042629	0.041078	0.038794
15.5			
16			
18.5			
25	0.036192		0.034733
25.5		0.034733	
40	0.028755	0.029097	0.02639
40.5			
41			
42.5			
59			
60		0.024406	0.021817
61	0.023103		
61.5			
62			
63.5			
78.5			
90	0.016705	0.01867	0.019292
91			

I-4 : MB concentration measurements at $u_f = 5\text{ cm/s}$ and $H = 11.2\text{ kA/m}$

Time (min)	Air flow velocity 0cm/s	Air flow velocity 0.27cm/s	Air flow velocity 0.68cm/s	Air flow velocity 1.172cm/s
0				
0.5	0.057295	0.058199	0.058018	0.059112
1	0.056399	0.056846	0.056756	0.057656
1.5		0.055333	0.05551	0.056399
2	0.054629	0.054454	0.054629	0.05551
2.5	0.053408	0.053408	0.053929	0.053929
3	0.052889	0.052889	0.053755	0.053581
4	0.050164	0.051603	0.052544	0.052889
5	0.049661		0.051688	0.051517
6				
7	0.047837	0.048662	0.049828	0.050501
8				
10	0.044921	0.045803	0.046612	0.047837
15	0.041309	0.041851		0.044204
15.5			0.042551	
16				
18.5				
25	0.036192	0.036929	0.03546	0.037671
25.5				
40	0.028414			0.031877
40.5			0.029441	
41				
42.5		0.031526		
59				
60	0.023427		0.024079	
61				0.025725
61.5				
62		0.023427		
63.5				
78.5				
90	0.018052	0.020547	0.020232	0.021498

APPENDIX J

CALCULATION OF DIFFUSION COEFFICIENT OF MB. INTO WATER

Wilke and Chang(1955) equation was used for the calculation of the diffusion coefficient of species A present in low concentration in species B. In our case, A represents MB (Methylene Blue) and B represents water. The equation is:

$$D_{AB} = 7.4 * 10^{-8} \frac{\sqrt{\phi_B M_B T}}{\mu_B V_A^{0.6}}$$

Where:

ϕ_B is the association factor for water=2.26[/]

M_B is the molecular weight of water = 18[g/mol]

T=298[K]

μ_B is water viscosity =1.0[Mpa.s]

V_A is the molar volume of MB = 457.1[cm^3 /mol]

Substituting the above values into equation above yields:

$$D_{AB} = 3.6 * 10^{-6} [cm^2 / s]$$